Eur. Phys. J. A (2023) 59:54
https://doi.org/10.1140/epja/s10050-023-00973-1

THE EUROPEAN PHYSICAL JOURNAL A

Regular Article -Theoretical Physics

The electromagnetic Sigma-to-Lambda transition form factors with coupled-channel effects in the space-like region

Yong-Hui Lin[1,a], **Hans-Werner Hammer**[2,3,b], **Ulf-G. Meißner**[1,4,5,c]

[1] Helmholtz-Institut für Strahlen- und Kernphysik and Bethe Center for Theoretical Physics, Universität Bonn, 53115 Bonn, Germany
[2] Technische Universität Darmstadt, Department of Physics, Institut für Kernphysik, 64289 Darmstadt, Germany
[3] ExtreMe Matter Institute EMMI and Helmholtz Forschungsakademie Hessen für FAIR (HFHF), GSI Helmholtzzentrum für Schwerionenforschung GmbH, 64291 Darmstadt, Germany
[4] Institut für Kernphysik, Institute for Advanced Simulation and Jülich Center for Hadron Physics, Forschungszentrum Jülich, 52425 Jülich, Germany
[5] Tbilisi State University, 0186 Tbilisi, Georgia

Received: 4 May 2022 / Accepted: 6 March 2023

Communicated by Che-Ming Ko

Abstract Using dispersion theory, the electromagnetic Sigma-to-Lambda transition form factors are expressed as the product of the pion electromagnetic form factor and the $\Sigma\bar{\Lambda} \to \pi\pi$ scattering amplitudes with the latter estimated from SU(3) chiral perturbation theory including the baryon decuplet as explicit degrees of freedom. The contribution of the $K\bar{K}$ channel is also taken into account and the $\pi\pi$–$K\bar{K}$ coupled-channel effect is included by means of a two-channel Muskhelishvili–Omnès representation. It is found that the electric transition form factor shows a significant shift after the inclusion of the $K\bar{K}$ channel, while the magnetic transition form factor is only weakly affected. However, the $K\bar{K}$ effect on the electric form factor is obscured by the undetermined coupling h_A in the three-flavor chiral Lagrangian. The error bands of the Sigma-to-Lambda transition form factors from the uncertainties of the couplings and low-energy constant in three-flavor chiral perturbation theory are estimated by a bootstrap sampling method.

1 Introduction

Electromagnetic form factors (EMFFs) give access to the strong interaction, which provides one of the most notorious challenges in the Standard Model due to the nonperturbative nature of Quantum Chromodynamics (QCD) at the low energy scale. On the one hand, the EMFFs can be extracted from a variety of experimental processes, such as lepton–hadron scattering, lepton–antilepton annihilation or radiative hadron decays. These EMFFs can be measured over a large energy range. On the other hand, dispersion theory, which is a powerful nonperturbative approach, allows for a theoretical description of the EMFFs. Consequently, the EMFFs are an ideal bridge between experimental measurements and theoretical studies of the low-energy strong interaction.

In the last decade, much research effort both in experiment and theory was focused on the nucleon EMFFs, largely triggered by the so-called proton radius puzzle [1]. For recent reviews, see e.g. Refs. [2–6]. In the process of unravelling this puzzle, dispersion theory has played and is playing a crucial role in the theoretical description of the nucleon EMFFs [7–10]. The dispersion theoretical parametrization of the nucleon EMFFs, first proposed in the early works [11–13] and further developed in Refs. [9,14,15], incorporates all constraints from unitarity, analyticity, and crossing symmetry, as well as the constraints on the asymptotic behavior of the form factors from perturbative QCD [16]. The state of the art of dispersive analyses of the nucleon EMFFs is reviewed in Ref. [17]. Very recently, all current measurements on electron-proton scattering, electron-positron annihilation, muonic hydrogen spectroscopy, and polarization measurements from Jefferson Laboratory could be consistently described in a dispersion theoretical analysis of the nucleon EMFFs [18].

The dispersive prescription of parameterizing the nucleon EMFFs can also be applied to other hadron states. The first two straightforward extensions concern the Delta baryon and the hyperon states, with the former obtained by flipping the spin of one of the quarks inside the nucleon and the latter by replacing one or several up or down quarks

[a] e-mail: yonghui@hiskp.uni-bonn.de (corresponding author)
[b] e-mail: Hans-Werner.Hammer@physik.tu-darmstadt.de
[c] e-mail: meissner@hiskp.uni-bonn.de

Published online: 21 March 2023

with one or more strange quarks. The EMFFs of the Delta and the hyperons provide complementary information about the intrinsic structure of the nucleon [19]. The electromagnetic properties of the Delta baryon have been studied in detail in Ref. [20]. Recent investigations of the hyperon EM structure are given in Refs. [19,21–26]. Ref. [19] considered once-subtracted dispersion relations for the electromagnetic Sigma-to-Lambda transition form factors (TFFs) and expressed these in terms of the pion EMFF and the two-pion-Sigma-Lambda scattering amplitudes. Using an Omnès representation, the pion EMFF could be expressed as the Omnès function of the pion P-wave phase shift which has been well determined from the Roy-type analyses of the pion-pion scattering amplitude [27]. An improved parameterization of the pion EMFF is also available, which includes further inelasticities and is applicable at higher energies [28]. Moreover, the two-pion-Sigma-Lambda scattering amplitudes could be calculated in a model-independent way by using three-flavor chiral perturbation theory (ChPT) [21]. Combining these studies and taking some reasonable values for couplings and the low-energy constants in three-flavor ChPT, the electromagnetic Sigma-to-Lambda TFFs were predicted in Ref. [19] where the pion rescattering and the role of the explicit inclusion of the decuplet baryons in three-flavor ChPT were also investigated.

In the present work, we extend the theoretical framework used in Ref. [19] to explore the effect of the $K\bar{K}$ inelasticity on the electromagnetic Sigma-to-Lambda transition form factors. This is performed by considering the two-channel Muskhelishvili-Omnès representation when introducing the pion rescattering effects. In principle, one should include even more inelasticities when implementing the dispersion theoretical parameterization for the Sigma-to-Lambda TFFs, as done in our previous work on the nucleon EMFFs [18]. However, it is difficult in the current case due to the poor data base which is required when constructing reliable inelasticities in the higher energy region, that is above the $K\bar{K}$ threshold at ~ 1 GeV. Note that the four-pion channel has negligible effects in the energy region around 1 GeV, see Ref. [29]. It is also known that the contribution of the four-pion channel to the pion and kaon form factors below 1 GeV is a three-loop effect in ChPT [30] and thus is heavily suppressed.

We remark that the 4π channel was shown to play an important role starting from 1.4 GeV in the S-wave case [31]. This is caused by the presence of the nearby scalar resonances $f_0(1370)$ and $f_0(1500)$ which were both observed to have a sizable coupling to four-pion states [32–34]. There is no evidence, however, for the presence of corresponding 1^- isovector states in the energy region of 1...2 GeV in the P-wave case. Moreover, another experimental finding of these references is that the 4π system likes to cluster into two resonances in the energy region above 1 GeV [31]. The lowest candidate is supposed to be the $\rho\rho$ channel for the P-wave isovector problem. From the phenomenological point of view, the inelasticity around 1 GeV should be saturated to a good approximation by the $\pi\pi$ and $K\bar{K}$ coupled-channel treatments in the P-wave case. Moreover, as we will show later, the effect of $K\bar{K}$ inelasticity is small. Thus, the relative ratio between the effects of the $K\bar{K}$ and four-pion channel could be enhanced. To investigate this relative ratio, a sophisticated calculation on the four-pion inelasticity is needed which goes beyond the present work.

In the present work, the $K\bar{K}$ inelasticity is implemented using SU(3) ChPT. The inclusion of the $K\bar{K}$ channel allows one to construct the Sigma-to-Lambda transition form factors up to 1 GeV precisely. In addition, the estimation of the theoretical uncertainties is improved by using the bootstrap approach [35].

The paper is organized as follows: In Sect. 2 we introduce the dispersion theoretical description of the electromagnetic Sigma-to-Lambda transition form factors and present the coupled-channel Muskhelishvili-Omnès representation for the inclusion of the $K\bar{K}$ inelasticity. Numerical results are collected in Sect. 3. The paper closes with a summary. Some technicalities are relegated to the appendix.

2 Formalism

Here, we discuss the basic formalism underlying our calculations. We first write down once-subtracted dispersion relations for the electric and magnetic Sigma-to-Lambda transition form factor and then discuss in detail their various ingredients, namely the vector form factor of the pion and the kaon and the amplitudes for $\Sigma^0\bar{\Lambda} \to \pi\pi$ and $\Sigma^0\bar{\Lambda} \to K\bar{K}$, in order.

2.1 Dispersion relations for the Sigma-to-Lambda TFFs

The electromagnetic Sigma-to-Lambda TFFs are defined as in Refs. [19,21],

$$\begin{aligned}&\langle\Sigma^0(p')|j^\mu|\Lambda(p)\rangle\\ &= e\,\bar{u}(p')\left(\left(\gamma^\mu + \frac{m_\Lambda - m_{\Sigma^0}}{t}\,q^\mu\right) F_1(t)\right.\\ &\left. + \frac{i\sigma^{\mu\nu}q_\nu}{m_\Lambda + m_{\Sigma^0}}\,F_2(t)\right)u(p)\,,\end{aligned} \tag{1}$$

with $t = (p' - p)^2 = q^2$ the four-momentum transfer squared. The scalar functions $F_1(t)$ and $F_2(t)$ are called the Dirac and Pauli transition form factors, respectively. One also writes the electric and magnetic Sachs transition form factors, given by the following linear combinations,

$$G_E(t) = F_1(t) + \frac{t}{(m_\Lambda + m_{\Sigma^0})^2}\,F_2(t),$$

$$G_M(t) = F_1(t) + F_2(t), \tag{2}$$

with the normalizations $F_1(0) = G_E(0) = 0$ and $F_2(0) = G_M(0) = \kappa \approx 1.98$. Here, κ is estimated from the experimental width of the decay $\Sigma^0 \to \Lambda\gamma$, see Ref. [19] for details. Unlike the nucleon case where one constructs dispersion relations for F_1 and F_2 [17], we work with the electric and magnetic Sachs form factors, i.e. G_E and G_M, for the Sigma-to-Lambda TFFs as in Ref. [19] since the Sigma-to-Lambda TFFs are of pure isovector type and the helicity decomposition used in Ref. [19] can easier be applied to the Sachs FFs.

In order to apply the spectral decomposition to estimate the imaginary part Im $G_{E/M}$, we consider the matrix element of the electromagnetic current Eq. (1) in the time-like region ($t > 0$), which is obtained via crossing symmetry,

$$\begin{aligned}
&\langle 0|j^\mu|\Sigma^0(p_3)\bar{\Lambda}(p_4)\rangle \\
&= e\,\bar{v}(p_4)\left(\left(\gamma^\mu + \frac{m_\Lambda - m_{\Sigma^0}}{t}(p_3+p_4)^\mu\right)F_1(t)\right. \\
&\left. - \frac{i\sigma^{\mu\nu}(p_3+p_4)_\nu}{m_\Lambda + m_{\Sigma^0}}F_2(t)\right)u(p_3)
\end{aligned} \tag{3}$$

where p_3 and p_4 are the momenta of the Σ^0 and $\bar{\Lambda}$ created by the electromagnetic current, respectively. The four-momentum transfer squared in the time-like region is then $t = (p_3 + p_4)^2$. With the $\pi\pi$ and $K\bar{K}$ inelasticities taken into account as depicted in Fig. 1, the unitarity relations for the Sigma-to-Lambda TFFs read [19,24,36,37],

$$\begin{aligned}
&\frac{1}{2i}\text{disc}_{\text{unit}}\, G_{E/M}(t) \\
&= \frac{1}{12\pi\sqrt{t}} \\
&\times\left(q_\pi^3(t)\,F_\pi^V(t)^*\,T_{E/M}^{\pi\pi}(t)\,\theta\left(t-4M_\pi^2\right)\right. \\
&\left. + 2q_K^3(t)\,F_K^V(t)^*\,T_{E/M}^{K\bar{K}}(t)\,\theta\left(t-4M_K^2\right)\right),
\end{aligned} \tag{4}$$

where

$$q_{\pi/K}(t) = \sqrt{\frac{\lambda(M_{\pi/K}^2, M_{\pi/K}^2, t)}{4t}} \tag{5}$$

is the center-of-mass momentum of the $\pi\pi/K\bar{K}$ two-body continuum with $\lambda(x,y,z) = x^2+y^2+z^2-2(xy+yz+zx)$ the Källén function. $F_{\pi/K}^V(t)$ is the vector-isovector form factor ($J = I = 1$) of the pion/kaon and $T_E^{\pi\pi}(t)$ and $T_M^{\pi\pi}(t)$ are two independent reduced P-wave $\Sigma^0\bar{\Lambda} \to \pi^+\pi^-$ amplitudes in the helicity basis. Similarly, $T_E^{K\bar{K}}(t)$ and $T_M^{K\bar{K}}(t)$ denote the corresponding reduced amplitudes for $\Sigma^0\bar{\Lambda} \to K^+K^-(K^0\bar{K}^0)$. Then the once-subtracted dispersion relations for the Sigma-to-Lambda TFFs are written as,

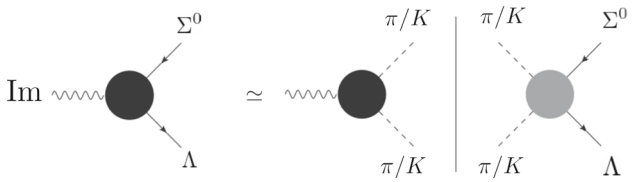

Fig. 1 The spectral decomposition of the matrix element of the electromagnetic current j_μ in Eq. (3)

$$\begin{aligned}
G_{E/M}(t) &= G_{E/M}(0) + \frac{t}{2\pi i}\int_{4M_\pi^2}^{\infty} dt' \frac{\text{disc}_{\text{unit}}\, G_{E/M}(t')}{t'(t'-t-i\epsilon)} \\
&+ G_{E/M}^{\text{anom}}(t)\,,
\end{aligned} \tag{6}$$

where the last term $G_{E/M}^{\text{anom}}(t)$ denotes the contribution of the anomalous cut which is non-zero when there exists an anomalous threshold in the involved processes [24,38–41]. This does happen when the $K\bar{K}$ channel is taken into account, see Appendix A for detailed discussions and the explicit expressions of the anomalous part. Next, we need to consider the various factors contributing to Eq. (6).

2.2 The $\Sigma^0\bar{\Lambda}$-$\pi\pi$ and $\Sigma^0\bar{\Lambda}$-$K\bar{K}$ amplitudes in the two-channel Muskhelishvili-Omnès representation

We start with the four-point amplitudes $\Sigma^0\bar{\Lambda} \to \pi^+\pi^-$ and $\Sigma^0\bar{\Lambda} \to K^+K^-$. Note that the matrix element Eq. (3), and also the four-point function $\Sigma^0\bar{\Lambda} \to \pi\pi$, can be written in the general form $\bar{v}_\Lambda(-p_z,\lambda)\Gamma u_{\Sigma^0}(p_z,\sigma)$ when one works in the center-of-mass frame and chooses the z-axis along the direction of motion of the Σ^0. Here, σ and λ are the helicities of the Σ^0 and $\bar{\Lambda}$ baryons, respectively. Due to parity invariance, there are only two non-vanishing terms, $\sigma = \lambda = +1/2$ and $\sigma = -\lambda = +1/2$. Concerning the matrix element Eq. (3), all components except for $\mu = 3$ vanish in the case of $\sigma = \lambda = +1/2$, that is,

$$\begin{aligned}
&\left\langle 0|j^3|\Sigma^0\left(p_z,\frac{1}{2}\right)\bar{\Lambda}\left(-p_z,\frac{1}{2}\right)\right\rangle \\
&= \bar{v}_\Lambda(-p_z,+1/2)\gamma^3 u_\Sigma(p_z,+1/2)G_E(t).
\end{aligned} \tag{7}$$

For $\sigma = -\lambda = +1/2$, only components related to $\mu = 1, 2$ survive:

$$\begin{aligned}
&\left\langle 0|j^1|\Sigma^0\left(p_z,\frac{1}{2}\right)\bar{\Lambda}\left(-p_z,-\frac{1}{2}\right)\right\rangle \\
&= \bar{v}_\Lambda(-p_z,-1/2)\gamma^1 u_\Sigma(p_z,+1/2)G_M(t),
\end{aligned} \tag{8}$$

and the matrix element for $\mu = 2$ differs from $\mu = 1$ only by a factor i. Equations (7) and (8) show that T_E in the imaginary part of G_E is only related to the amplitude component $\mathcal{M}^{\Sigma\bar{\Lambda}\to\pi\pi/K\bar{K}}(+1/2,+1/2)$ while T_M comes from

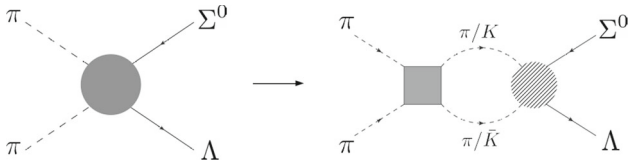

Fig. 2 The four-point function $\pi\pi \to \Sigma^0 \bar{\Lambda}$ including two-pion rescattering. The hatched circle is the part containing only left-hand cuts and a polynomial

$\mathcal{M}^{\Sigma\bar{\Lambda}\to\pi\pi/K\bar{K}}(+1/2,-1/2)$. Then we define the reduced amplitudes $T_{E/M}$ as [19,42]

$$\begin{aligned}&\mathcal{M}^{\Sigma\bar{\Lambda}\to\pi\pi/K\bar{K}}(t,\theta,+1/2,+1/2)\\&=\bar{v}_\Lambda(-p_z,+1/2)\gamma^3 u_\Sigma(p_z,+1/2)q_{\pi/K}T_E^{\pi/K}(t)d^1_{0,0}(\theta)\\&+\text{other partial waves with } J\neq 1\,,\end{aligned}\tag{9}$$

$$\begin{aligned}&\mathcal{M}^{\Sigma\bar{\Lambda}\to\pi\pi/K\bar{K}}(t,\theta,+1/2,-1/2)\\&=-\sqrt{2}\bar{v}_\Lambda(-p_z,-1/2)\gamma^1 u_\Sigma(p_z,+1/2)q_{\pi/K}T_M^{\pi/K}(t)d^1_{1,0}(\theta)\\&+\text{other partial waves with } J\neq 1\,,\end{aligned}\tag{10}$$

where $d^1_{1/2\pm1/2,0}(\theta)$ is the Wigner d-matrix. Finally, we obtain

$$T_E^{\pi/K}(t)=\frac{3}{2}\int_0^\pi d\theta\,\sin\theta\,\frac{\mathcal{M}^{\Sigma\bar{\Lambda}\to\pi\pi/K\bar{K}}(t,\theta,+1/2,+1/2)}{\bar{v}_\Lambda(-p_z,+1/2)\,\gamma^3\,u_\Sigma(p_z,+1/2)\,q_{\pi/K}}\cos\theta\,,\tag{11}$$

$$T_M^{\pi/K}(t)=\frac{3}{4}\int_0^\pi d\theta\,\sin\theta\,\frac{\mathcal{M}^{\Sigma\bar{\Lambda}\to\pi\pi/K\bar{K}}(t,\theta,+1/2,-1/2)}{\bar{v}_\Lambda(-p_z,-1/2)\,\gamma^1\,u_\Sigma(p_z,+1/2)\,q_{\pi/K}}\sin\theta\,.\tag{12}$$

As done in Ref, [19], the pion rescattering effect can be introduced into $T_{E/M}$ via the Muskhelishvili-Omnès equation that is shown in Fig. 2. With the inclusion of the $K\bar{K}$ channel, the two-channel Muskhelishvili-Omnès representation reads [43–46]

$$\begin{aligned}\mathbf{T}_{E/M}(t)&=\mathbf{K}_{E/M}(t)+\mathbf{T}^{\text{anom}}_{E/M}(t)\\&+\boldsymbol{\Omega}(t)\left(\mathbf{P}_{0,E/M}(t)-\frac{t}{\pi}\int_{4M_\pi^2}^\infty dt'\frac{[\text{Im}\boldsymbol{\Omega}^{-1}(t')]\mathbf{K}_{E/M}(t')}{t'(t'-t-i\epsilon)}\right),\end{aligned}\tag{13}$$

with $\mathbf{T}=\left(T_\pi,\sqrt{2}T_K\right)^T$, $\mathbf{P}_0=\left(P_{0,\pi},\sqrt{2}P_{0,K}\right)^T$ and $\mathbf{K}=\left(K_\pi,\sqrt{2}K_K\right)^T$.[1] $\boldsymbol{\Omega}(t)$ is the two-dimension Omnès matrix for the P-wave isovector $\pi\pi$–$K\bar{K}$ coupled-channel system. $\mathbf{T}^{\text{anom}}_{E/M}(t)$ again indicates the anomalous contribution and its explicit formula is given in Appendix. A. The $K_{\pi/K}$ denotes the part of the $\Sigma\bar{\Lambda}\to\pi\pi/K\bar{K}$ amplitude that only contains the left-hand cut (LHC) and P_0 is the remainder which is purely polynomial. Therefore, $K_{\pi/K}$ and $P_{0,\pi/K}$ are given by

$$K_E(t)=\frac{3}{2}\int_0^\pi d\theta\,\sin\theta\,\frac{\mathcal{M}^{\text{pole}}(t,\theta,+1/2,+1/2)}{\bar{v}_\Lambda(-p_z,+1/2)\,\gamma^3\,u_\Sigma(p_z,+1/2)\,q_{\pi/K}}\cos\theta\,,\tag{14}$$

$$P_0^E(t)=\frac{3}{2}\int_0^\pi d\theta\,\sin\theta\,\frac{\mathcal{M}^{\text{contact}}(t,\theta,+1/2,+1/2)}{\bar{v}_\Lambda(-p_z,+1/2)\,\gamma^3\,u_\Sigma(p_z,+1/2)\,q_{\pi/K}}\cos\theta\,,\tag{15}$$

with $\mathcal{M}^{\Sigma\bar{\Lambda}\to\pi\pi/K\bar{K}}(t,\theta)=\mathcal{M}^{\text{pole}}+\mathcal{M}^{\text{contact}}$. The magnetic parts are derived equivalently from Eq. (12),

$$K_M(t)=\frac{3}{4}\int_0^\pi d\theta\,\sin\theta\,\frac{\mathcal{M}^{\text{pole}}(t,\theta,+1/2,-1/2)}{\bar{v}_\Lambda(-p_z,-1/2)\,\gamma^1\,u_\Sigma(p_z,+1/2)\,q_{\pi/K}}\sin\theta\,,\tag{16}$$

$$P_0^M(t)=\frac{3}{4}\int_0^\pi d\theta\,\sin\theta\,\frac{\mathcal{M}^{\text{contact}}(t,\theta,+1/2,-1/2)}{\bar{v}_\Lambda(-p_z,-1/2)\,\gamma^1\,u_\Sigma(p_z,+1/2)\,q_{\pi/K}}\sin\theta\,.\tag{17}$$

All the reduced amplitudes $K_{\pi/K}$ and $P_{0,\pi/K}$ are calculated up to next-to-leading order (NLO) within the framework of the three-flavor baryon ChPT that includes the decuplet baryon as explicit degrees of freedom. Their explicit expressions are derived in detail in Appendix B.

2.3 The P-wave Omnès matrix and π, K vector form factors

In this subsection, we derive the P-wave isovector Omnès matrix and solve for the pion and kaon EMFFs in the coupled-channel formalism. $\boldsymbol{\Omega}$ satisfies the unitarity relation [46]

$$\frac{1}{2i}\text{disc}\,\Omega_{ij}=(t_1^1)^*_{im}\Sigma_m\Omega_{mj}\,,\tag{18}$$

where

$$\boldsymbol{\Sigma}(t)=\text{diag}\left(\sigma_\pi q_\pi^2\theta(t-4M_\pi^2),\sigma_K q_K^2\theta(t-4M_K^2)\right)\tag{19}$$

with

$$\sigma_{\pi/K}(t)=\sqrt{1-\frac{4M^2_{\pi/K}}{t}}\tag{20}$$

[1] $\mathbf{K}=\left(K_\pi\theta(t'-4M_\pi^2),\sqrt{2}K_K\theta(t'-4M_K^2)\right)^T$ is implicit in the integrand $[\text{Im}\boldsymbol{\Omega}^{-1}(t')]\mathbf{K}(t')$.

is the diagonal phase space matrix. The $J = I = 1$ $\pi\pi$–$K\bar{K}$ coupled-channel T-matrix $\mathbf{t}_1^1$ is parameterized as

$$\mathbf{t}_1^1 = \begin{pmatrix} \dfrac{\eta e^{2i\delta_1^1} - 1}{2i\sigma_\pi q_\pi^2} & g e^{i\psi} \\ g e^{i\psi} & \dfrac{\eta e^{2i(\psi-\delta_1^1)} - 1}{2i\sigma_K q_K^2} \end{pmatrix} . \tag{21}$$

where g and ψ are the modulus and phase of the P-wave isovector $\pi\pi \to K\bar{K}$ scattering amplitude, respectively. The inelasticity η is defined by

$$\eta(t) = \sqrt{1 - 4\sigma_\pi \sigma_K (q_\pi q_K)^2 g^2 \theta(t - 4M_K^2)}. \tag{22}$$

Then we can write the dispersion relation for the Omnès matrix $\boldsymbol{\Omega}$ as

$$\Omega_{ij}(t) = \frac{1}{2\pi i} \int_{4M_\pi^2}^{\infty} \mathrm{d}z \frac{\mathrm{disc}\ \Omega_{ij}(z)}{z - t - i\epsilon} . \tag{23}$$

The analytic solution of the integral equation Eq. (23) was given in Ref. [47] for the single-channel problem. However, there are no known analytic solutions for two or more channel cases where one has to construct the solutions numerically, either by an iterative procedure [48] or a discretization method [31]. Here, we adopt the iterative approach to solve the P-wave $\pi\pi$–$K\bar{K}$ coupled-channel Omnès matrix. Substituting Eq. (18) into Eq. (23), one obtains a two-dimensional system of integral equations

$$\begin{cases} \mathrm{Re}\ \chi_1(t) = \dfrac{1}{\pi} \mathcal{P} \displaystyle\int_{4M_\pi^2}^{\infty} \mathrm{d}z \frac{\mathrm{Im}\chi_1(z)}{z - t} , \\ \mathrm{Re}\ \chi_2(t) = \dfrac{1}{\pi} \mathcal{P} \displaystyle\int_{4M_\pi^2}^{\infty} \mathrm{d}z \frac{\mathrm{Im}\chi_2(z)}{z - t} , \end{cases} \tag{24}$$

where

$$\begin{aligned} \mathrm{Im}\chi_1(z) &= \mathrm{Re}\left[(t_1^1)_{11}^* \Sigma_1 \chi_1 \right] + \mathrm{Re}\left[(t_1^1)_{12}^* \Sigma_2 \chi_2 \right] , \\ \mathrm{Im}\chi_2(z) &= \mathrm{Re}\left[(t_1^1)_{21}^* \Sigma_1 \chi_1 \right] + \mathrm{Re}\left[(t_1^1)_{22}^* \Sigma_2 \chi_2 \right] , \end{aligned} \tag{25}$$

and $\mathcal{P}$ denotes the principal value. Searching for solutions of $\boldsymbol{\Omega}(t)$ is equivalent to searching for two independent solutions of the integral equation set for the two-dimensional array $(\chi_1, \chi_2)^T$. Using the iterative procedure, one can obtain a series of solutions $(\chi_1^\lambda, \chi_2^\lambda)^T$ starting with various initial inputs $\chi_1(t) = 1$, $\chi_2(t) = \lambda$, where λ is a real parameter. Note that the iterative process is linear and the results of the iteration is therefore a linear function of λ [48]. Then the solution family $\{(\chi_1^\lambda, \chi_2^\lambda)^T\}$ contains only two linearly independent members. Here, we take the same convention as Ref. [46] to construct two independent solutions, $(\Omega_{11}, \Omega_{21})^T$ and $(\Omega_{12}, \Omega_{22})^T$, that satisfy the normalizations

$$\Omega_{11}(0) = \Omega_{22}(0) = 1 \ \text{ and } \ \Omega_{12}(0) = \Omega_{21}(0) = 0 ,$$

from two arbitrary solutions $(\chi_1^{\lambda_1}, \chi_2^{\lambda_1})^T$ and $(\chi_1^{\lambda_2}, \chi_2^{\lambda_2})^T$.

With the two-channel Muskhelishvili-Omnès representation, the binary function composed of the vector FFs of the pion and the kaon fulfills the same unitarity relation Eq. (18). Then one can solve the pion and kaon vector form factors

$$\begin{pmatrix} F_\pi^V(t) \\ \sqrt{2} F_K^V(t) \end{pmatrix} = \begin{pmatrix} \Omega_{11}(t) & \Omega_{12}(t) \\ \Omega_{21}(t) & \Omega_{22}(t) \end{pmatrix} \begin{pmatrix} F_\pi^V(0) \\ \sqrt{2} F_K^V(0) \end{pmatrix} , \tag{26}$$

which are normalized as $F_\pi^V(0) = 1$ and $F_K^V(0) = 1/2$.

To solve the $J = I = 1$ $\pi\pi$–$K\bar{K}$ Omnès matrix, the required input is the P-wave isovector $\pi\pi$–$K\bar{K}$ scattering matrix $\mathbf{t}_1^1$, i.e. Equation (21), that is constructed from the $\pi\pi$ P-wave isovector phase shift δ_1^1, the modulus g and phase ψ of the P-wave isovector $\pi\pi \to K\bar{K}$ amplitude. The phase shift δ_1^1 up to 1.4 GeV was extracted precisely from the Roy-type analyses of the pion-pion scattering amplitude in Ref. [27]. We take the same prescription as in Ref. [28] to extrapolate it smoothly to reach π at infinity. Then $\delta_1^1(t)$ is given by

$$\delta_1^1(t) = \begin{cases} 0, & 0 \le \sqrt{t} \le 2M_\pi , \\ \delta_{f_1}(t), & 2M_\pi < \sqrt{t} \le 2M_K , \\ \delta_{f_2}(t), & 2M_K < \sqrt{t} \le \sqrt{t_0} , \\ \delta_{f_3}(t), & \sqrt{t_0} < \sqrt{t} , \end{cases} \tag{27}$$

where

$$\begin{aligned} \delta_{f_1}(t) &= \cot^{-1}\left(\frac{\sqrt{t}}{2q_\pi^3} (M_\rho^2 - t) \left(\frac{2M_\pi^3}{M_\rho^2 \sqrt{t}} + 1.043 \right.\right. \\ &\quad \left.\left. + 0.19 \frac{\sqrt{t} - \sqrt{t_1 - t}}{\sqrt{t} + \sqrt{t_1 - t}} \right) \right) , \\ \delta_{f_2}(t) &= \delta_{f_1}(4M_K^2) + 1.39 \left(\frac{\sqrt{t}}{2M_K} - 1 \right) - 1.7 \left(\frac{\sqrt{t}}{2M_K} - 1 \right)^2 , \\ \delta_{f_3}(t) &= \pi + (\delta_{f_2}(t_0) - \pi) \left(\frac{t_2 + t_0}{t_2 + t} \right) . \end{aligned} \tag{28}$$

Here, $t_0 = (1.4\ \mathrm{GeV})^2$, $t_1 = (1.05\ \mathrm{GeV})^2$ and $t_2 = (10\ \mathrm{GeV})^2$.

The P-wave $\pi\pi \to K\bar{K}$ amplitude up to $\sqrt{t_3} = 1.57$ GeV is taken from Ref. [49] where the modulus g in the region of $4M_\pi^2 ... 4M_K^2$ was solved from the Roy-Steiner equation with the experimental data of P-wave $\pi\pi \to K\bar{K}$ scattering [50,51] above the $K\bar{K}$ threshold as input, while the phase ψ was fitted to experimental data [50,51]. Note that the two-channel Muskhelishvili-Omnès representation in terms of $\pi\pi$ and $K\bar{K}$ intermediate states should only work well in the lower energy region [46]. Further, the asymptotic values of phase shifts in the coupled-channel systems have to satisfy

$$\lim_{t\to\infty} \sum \delta_l^I(t) \ge n\pi, \tag{29}$$

to ensure that the system of integral equations, Eq. (24), has a unique solution [31,52]. n is the number of channels that are considered in the formalism. It requires $\psi = \delta_{1,\pi\pi}^1 +$

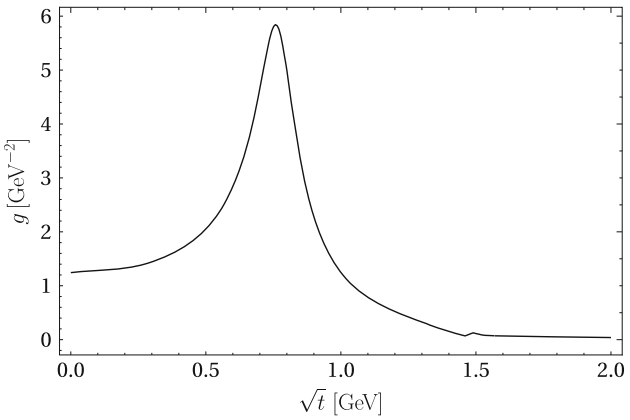

Fig. 3 The modulus g of the P-wave $\pi\pi \to K\bar{K}$ amplitude given by Ref. [49]

$\delta^1_{1,K\bar{K}} \geq 2\pi$ in Eq. (21). g and ψ are extrapolated smoothly to 0 and 2π by means of [31]

$$\psi(t) = 2\pi + (\psi(t_4) - 2\pi)\,\hat{f}\left(\frac{t}{t_4}\right),$$
$$g(t) = g(t_3)\,\hat{f}\left(\frac{t}{t_3}\right), \quad \text{with } \hat{f}(x) = \frac{2}{1+x^{3/2}}. \tag{30}$$

where the extrapolation point t_4 of ψ should be far away from 1.5 GeV since there is a structure located around 1.5 GeV in the phase of the P-wave $\pi\pi \to K\bar{K}$ amplitude. Here we take the value $\sqrt{t_4} = 5$ GeV for ψ. Such a structure should also leave trails in the modulus g. However, only g up to $\sqrt{2}$ GeV is estimated in Ref. [49] and a small bump around 1.5 GeV in g is only reflected roughly by several data points above 1.4 GeV measured by Ref. [50], see Fig. 9 in Ref. [49]. The modulus used in our work is presented in Fig. 3, while the δ^1_1 and ψ are presented when we show the solved pion and kaon vector form factors.

The obtained Ω matrix elements are presented in Fig. 4. The pion and kaon vector form factors calculated from Eq. (26) are then given in Fig. 5. Clearly, one can see from Fig. 5 that the phase of F^V_π and F^V_K are consistent with the input $\pi\pi$ phase shift δ^1_1 and the phase ψ of the P-wave $\pi\pi \to K\bar{K}$ scattering amplitude respectively, which is similar with the finding for the S-wave case by Ref. [46].

3 Results

Using the reduced amplitudes $P^{E/M}_{0,\pi/K}$ and $K^{E/M}_{\pi/K}$ given in Appendix B and the anomalous expressions presented in Appendix A, we can now calculate the amplitudes $T^{\pi/K}_{E/M}$ in Eq. (4) including $\pi\pi/K\bar{K}$ rescattering effects from Eq. (13). Finally, we calculate the Sigma-to-Lambda transition form factors $G_{E/M}$ from the dispersion relations Eq. (6). Two issues remain to be clarified. First, we have to fix all the couplings in the expressions of $P^{E/M}_{0,\pi/K}$ and $K^{E/M}_{\pi/K}$. These are

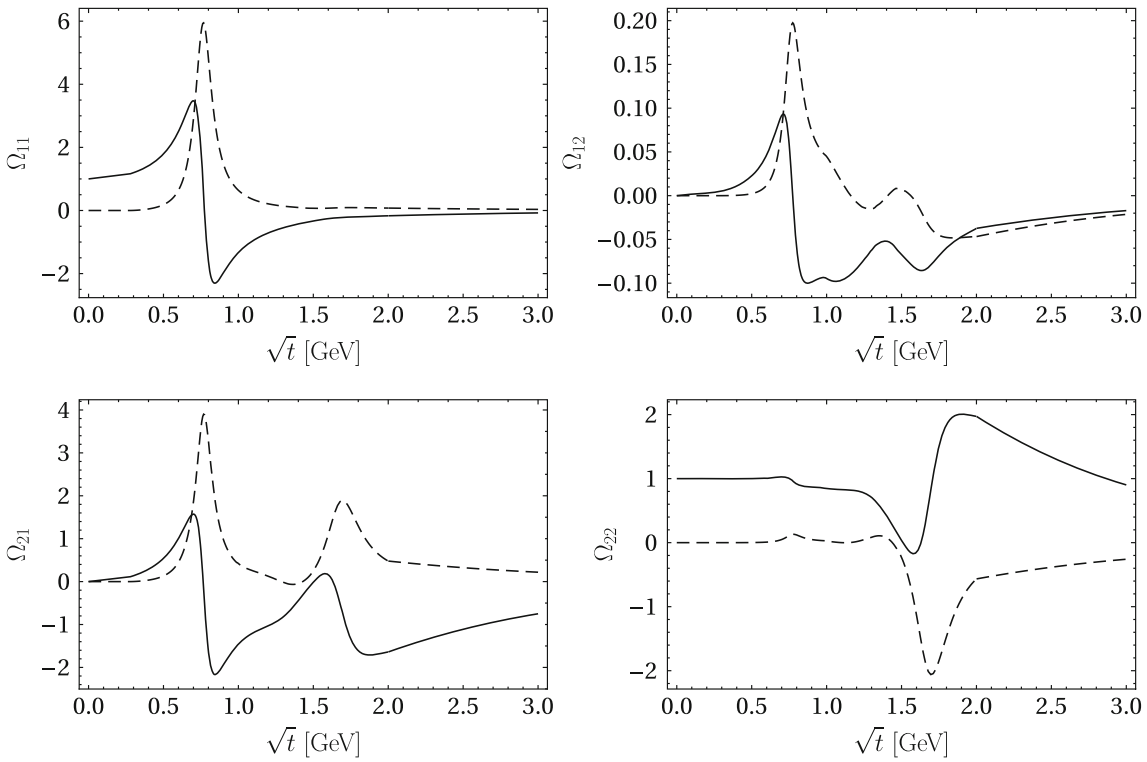

Fig. 4 Real (solid line) and imaginary (dashed line) parts of the Omnès matrix elements Ω

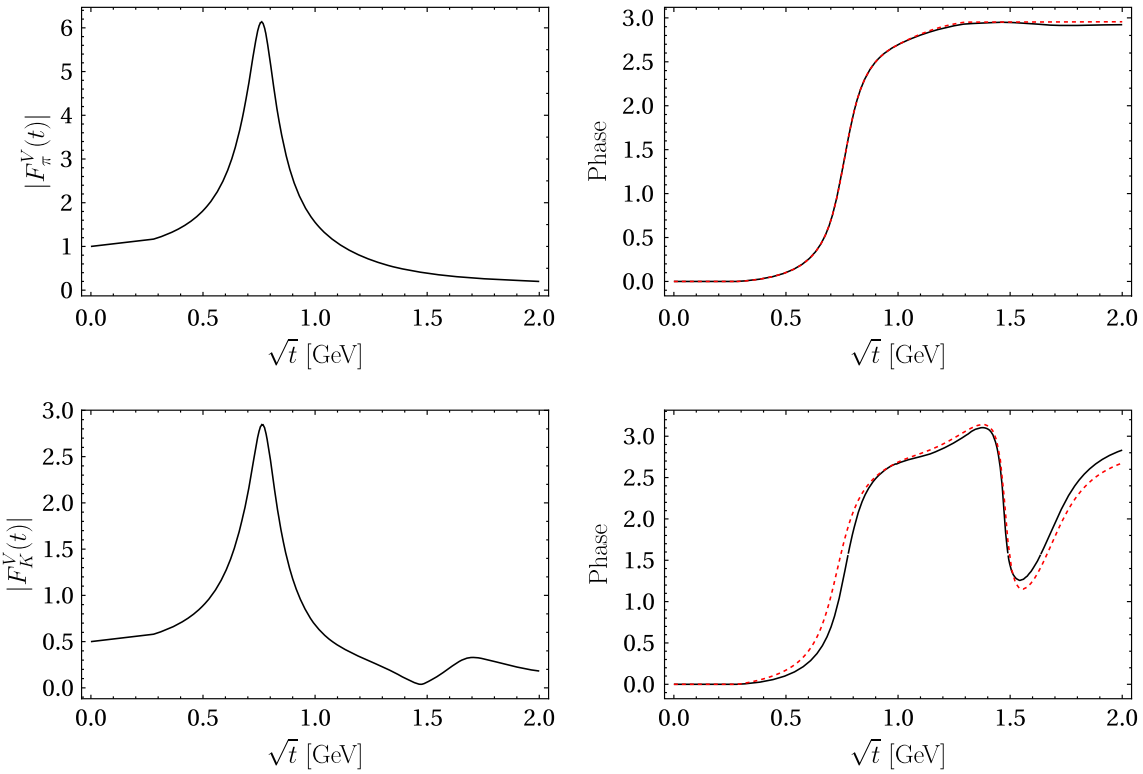

Fig. 5 Modulus (left) and phase (right) of the vector pion (upper) and kaon (lower) form factors given by Eq. (26). The input $\pi\pi$ phase shift δ_1^1 (upper) and phase ψ (lower) of the P-wave isovector $\pi\pi \to K\bar{K}$ amplitude are also presented as the red-dashed lines for comparison. Note that the asymptotic values of δ_1^1 and ψ are π and 2π respectively. The latter is invisible in the plot since its extrapolation point is set as 5 GeV

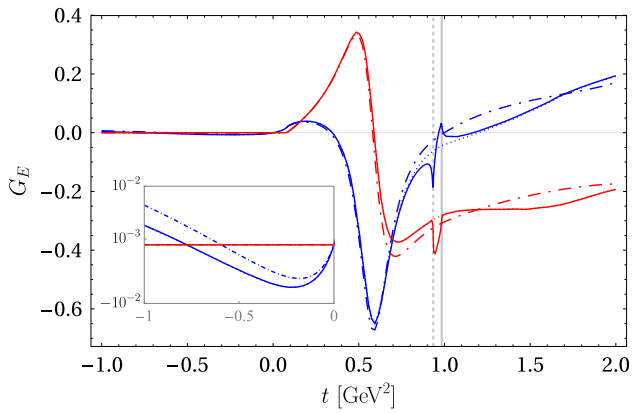

Fig. 6 The imaginary (red) and real (blue) part of the electric transition form factor G_E. The dash-dotted, dotted, solid lines denote the results within the single $\pi\pi$ channel, $\pi\pi$–$K\bar{K}$ coupled channel without and with the anomalous contribution scenarios, respectively, when $F_\Phi = 100$ MeV, $b_{10} = 1.06$ GeV^{-1}, $h_A = 2.22$ and $\Lambda = 1.5$ GeV. The vertical dashed and solid lines represent respectively the anomalous threshold (Eq. (36)) and the $K\bar{K}$ threshold

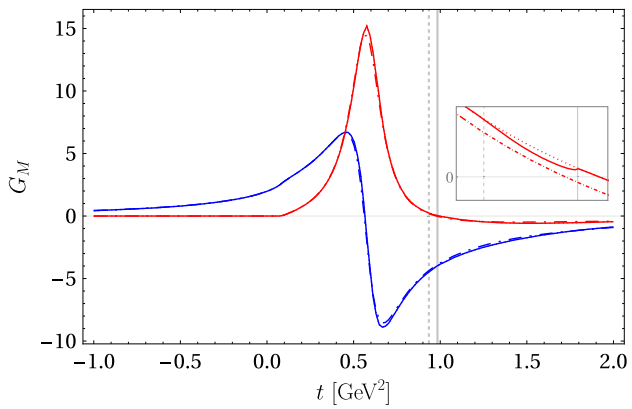

Fig. 7 The imaginary (red) and real (blue) part of the magnetic transition form factor G_M. For notations, see Fig. 6

D, F, F_Φ for the LO octet-to-octet interactions, h_A for the LO decuplet-to-octet interaction, and b_{10} for the NLO octet-to-octet interaction. In ChPT, D and F are well constrained around 0.8 and 0.5, respectively. Here we use $D = 0.80$, $F = 0.46$ [21]. In SU(3) ChPT, F_Φ can take three different values at LO, namely $F_\pi = 92.4$ MeV, $F_K = 113.0$ MeV and $F_\eta = 120.1$ MeV [53]. Often, one chooses the average of these, that is, $F_\Phi = (F_\pi + F_K + F_\eta)/3$. Here, we take $F_\Phi = 100 \pm 10$ MeV to cover mainly the π and K contributions. h_A can be determined from the experimental widths of either $\Sigma^* \to \Lambda\pi$ or $\Sigma^* \to \Sigma\pi$. We take the value $h_A = 2.3 \pm 0.3$ [19], here an additional 10% error

is added to account for the SU(3) flavor symmetry breaking effect when applied to the vertices involving a Ξ^*. The low-energy constant b_{10} was estimated in Ref. [54] based on the resonance saturation hypothesis as $b_{10} = 0.95\ \text{GeV}^{-1}$. A larger value $b_{10} = 1.24\ \text{GeV}^{-1}$ is used in Ref. [21]. A very recent determination based on the ChPT fits to lattice data of the axial-vector currents of the octet baryons gives $b_{10} = 0.76\,\text{GeV}^{-1}$ [55]. Taking all these determinations into account, $b_{10} = (1.0 \pm 0.3)\ \text{GeV}^{-1}$ is used here. Second, we introduce an energy cutoff Λ in the integration along the unitarity cut in Eq. (6) and Eq. (13). We consider two values for the cutoff, $\Lambda = 1.5$ and 2.0 GeV, to check the sensitivity of our results to it.

Now we are in the position to present our numerical results for the electromagnetic Sigma-to-Lambda transition form factors. First, we present the electric transition form factor G_E obtained with the radius-adjusted parameters given in Ref. [19], i.e. $F_\Phi = 100$ MeV, $b_{10} = 1.06\ \text{GeV}^{-1}$ and $h_A = 2.22$ where the radius is adjusted to the fourth-order ChPT result from Ref. [21], in Fig. 6. Note that $\Lambda = 1.5$ GeV is used in these calculations. The result from the single $\pi\pi$ channel consideration is also plotted for an intuitive comparison. Taking the same parameter values, we find good agreement with Ref. [19]. After the inclusion of the $K\bar{K}$ inelasticity, a logarithmic singularity located at the anomalous threshold $t_- = 0.935$ GeV in the unphysical area of the time-like region is introduced into the TFF G_E. Moreover, additional nonzero imaginary parts along the anomalous cut are produced for the TFFs by Eq. (42) and Eq. (43). This is similar to the triangle singularity mechanism that leads to a quasi-state phenomenon in the physical observables [56], except the anomalous threshold here can not be accessed directly by the experiments. The imaginary parts of G_E in the space-like region, however, are still zero since the nonzero contributions from Eq. (42) are exactly canceled by those from the unitarity integral of Eq. (43).

A similar plot for the magnetic TFF G_M is shown in Fig. 7 where there is a cusp-like structure rather than a logarithmic singularity in G_E located at the anomalous threshold since the coefficient f in Eq. (39) which is proportional to $(Y^2 - \kappa^2)$ does vanish at the anomalous threshold for G_M. Note that such cusp-like structure is almost invisible due to the large scale variation of the magnitude of G_M. With that set of parameters, a 52% decrease is produced by the $K\bar{K}$ channel for G_E at $t = -1\ \text{GeV}^2$,[2] while only a 3% decrease happens for G_M. One should be aware, however, of the large difference between the effects of $K\bar{K}$ channel in G_E and G_M is the result of the much larger magnitude that G_M has overall than G_E. The absolute effect of the $K\bar{K}$ inelasticity in G_M is actually of compatible size as in G_E (sometimes even larger).

In Fig. 8, we show the electric transition form factor G_E between the estimation including only the $\pi\pi$ intermediate state and the $\pi\pi$–$K\bar{K}$ coupled-channel determination with errors. Note that the TFFs are real-valued in the space-like region. The solid curves are calculated again with the radius-adjusted parameters. The error bands in Fig. 8 are estimated by the bootstrap sampling over the three-dimensional parameter space that is spanned by F_Φ, b_{10} and h_A. Note that the electric form factor is independent of the low-energy constant b_{10}, see the expressions in Appendix B. As in Ref. [19], the uncertainty in h_A gives the dominant contribution. The effect on G_E introduced by the inclusion of the $K\bar{K}$ inelasticity is heavily intertwined with the large uncertainties from the variation of h_A and Λ. Overall, the role of the cutoff is a bit more complicated than in the single $\pi\pi$ channel case. The situation is different for G_M which is displayed in Fig. 9. The magnetic Sigma-to-Lambda transition form factor G_M is almost unchanged after including the $K\bar{K}$ inelasticity. Moreover, G_M has much larger absolute errors from the bootstrap method. At $t = -1\ \text{GeV}^2$, the bootstrap uncertainty from F_Φ, h_A and b_{10} is already of order ± 1, dominated by the uncertainty in b_{10}. As in Ref. [19], we find a very small sensitivity of G_M to the variation of the cutoff Λ. In addition to providing valuable insights into the electromagnetic structure of hyperons, experimental data for the transition form factors may thus also help to constrain these parameters.

4 Summary

In this paper, we extended the dispersion theoretical determination of the electromagnetic Sigma-to-Lambda transition form factors presented in Ref. [19] from the $\pi\pi$ intermediate state to the $\pi\pi$–$K\bar{K}$ coupled-channel configuration within the SU(3) ChPT framework. After including the $K\bar{K}$ channel, a shift of the electric Sigma-to-Lambda transition form factor G_E is presented, while the magnetic form factor G_M stays essentially unchanged. At present, the dispersion theoretical determination of electromagnetic Sigma-to-Lambda transition form factors suffers from sizeable uncertainties due to the poor knowledge of the LEC b_{10} and coupling h_A. The precise determination of this three-flavor LEC from the future experiments will be helpful to pin down the hyperon TFFs. In a next step, it will be of interest to explore the elastic hyperon electromagnetic form factors based on the theoretical framework that combines dispersion theory and three-flavor chiral perturbation theory.

Acknowledgements YHL is grateful to Meng-Lin Du, De-Liang Yao and Feng-Kun Guo for many valuable discussions. YHL thanks also Yu-Ji Shi for some discussions on the kaon vector form factors. This

[2] Note that G_E is overall very small, as is expected due to the vanishing overall charge of the Λ and Σ^0.

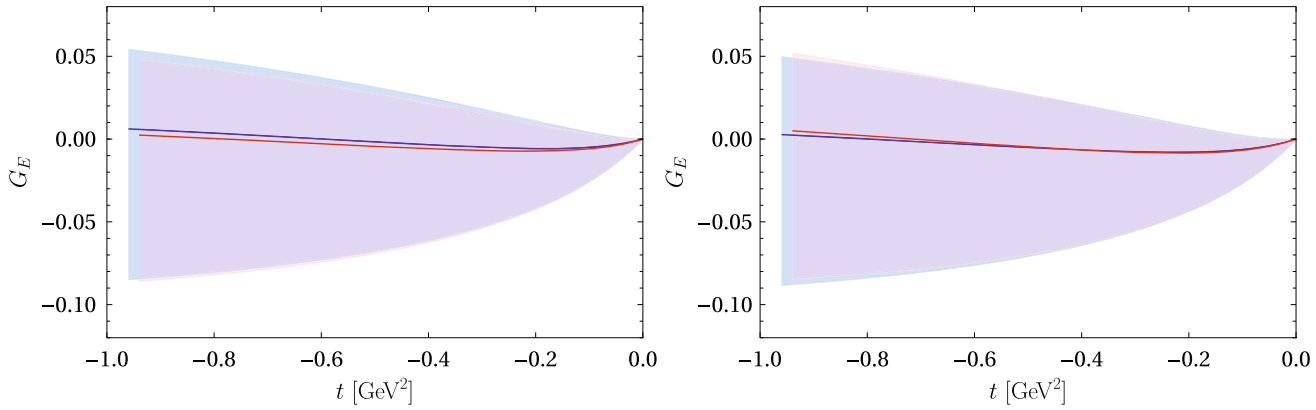

Fig. 8 The electric transition form factor G_E obtained from the once-subtracted dispersion relation Eq. (6) with an energy cutoff $\Lambda = 1.5$ GeV (left) and 2.0 GeV (right). The blue lines denote the results from the single $\pi\pi$ channel consideration as in Ref. [19] and the red lines are those after including the $K\bar{K}$ channel. The error bands are estimated based on bootstrap sampling

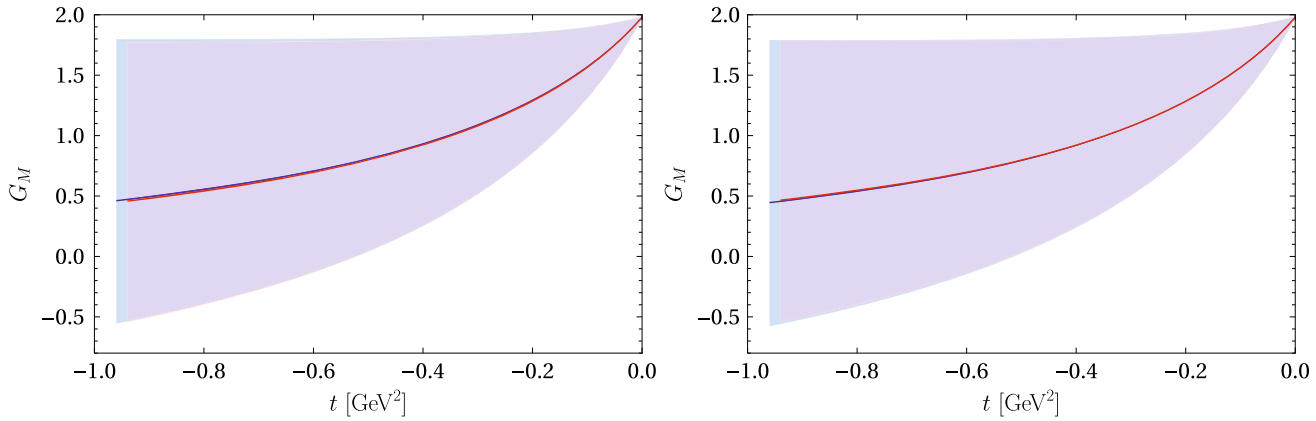

Fig. 9 The magnetic transition form factor G_M obtained from the once-subtracted dispersion relation Eq. (6) with an energy cutoff $\Lambda = 1.5$ GeV (left) and 2.0 GeV (right). For notations, see Fig. 8

work of UGM and YHL is supported in part by the DFG (Project number 196253076—TRR 110) and the NSFC (Grant no. 11621131001) through the funds provided to the Sino-German CRC 110 "Symmetries and the Emergence of Structure in QCD", by the Chinese Academy of Sciences (CAS) through a President's International Fellowship Initiative (PIFI) (Grant no. 2018DM0034), by the VolkswagenStiftung (Grant No. 93562), and by the EU Horizon 2020 research and innovation programme, STRONG-2020 project under grant agreement No 824093. HWH was supported by the Deutsche Forschungsgemeinschaft (DFG, German Research Foundation)—Projektnummer 279384907—CRC 1245 and by the German Federal Ministry of Education and Research (BMBF) (Grant no. 05P21RDFNB).

Funding Information Open Access funding enabled and organized by Projekt DEAL.

Data Availability Statement This manuscript has no associated data or the data will not be deposited. [Authors' comment: This is a theoretical paper without experimental data and all numerical results can be reproduced using the information presented above.]

A Unitarity relations and the anomalous pieces

Let us start from the single channel case. The unitarity relations for the Σ-to-Λ TFFs $G_{E/M}$ (in the followings we drop the index E/M) within the single $\pi\pi$ channel assumption read [19,24]

$$\frac{1}{2i}\text{disc}_{\text{unit}}\, G(t) = \frac{1}{24\pi} T_\pi \Sigma_\pi F_\pi^{V*}\,, \tag{31}$$

where $\Sigma_\pi = \sigma_\pi q_\pi^2$ with σ and q defined by Eq. (20) and Eq. (5) respectively, and $q = \sqrt{t}\sigma/2$. Moving to the $\pi\pi$–$K\bar{K}$ coupled-channel case, one first considers the vector pion and kaon form factors; they satisfy the unitarity relations [46,57],

$$\frac{1}{2i}\text{disc}\,\mathbf{F}^V(t) = \mathbf{t}_1^{1*}\boldsymbol{\Sigma}\mathbf{F}^V, \quad \mathbf{F}^V = \left(F_\pi^V,\ \sqrt{2}F_K^V\right)^T. \tag{32}$$

Similarly, the $\Sigma^0\bar{\Lambda} \to \pi\pi$ and $\Sigma^0\bar{\Lambda} \to K\bar{K}$ P-wave amplitudes fulfill the unitarity relations

$$\frac{1}{2i}\text{disc}\,\mathbf{T}(t) = \mathbf{t}_1^{1*}\boldsymbol{\Sigma}\mathbf{T}, \quad \mathbf{T} = \left(T_\pi,\ \sqrt{2}T_K\right)^T. \tag{33}$$

The key information that the above two equations provide us is the relative ratio between the $\pi\pi$ and $K\bar{K}$ channels in the $J = I = 1$ coupled-channel problem. Then with the single-$\pi\pi$ unitarity relations at hand already, that is, Eq. (31), one can easily extend to the two-channel case:

$$\begin{aligned}\frac{1}{2i}\text{disc}_{\text{unit}}\,G(t) &= \frac{1}{24\pi}\mathbf{T}^T\boldsymbol{\Sigma}\mathbf{F}^{V*}\\ &= \frac{1}{24\pi}\left(T_\pi,\ \sqrt{2}T_K\right)\cdot\begin{pmatrix}\Sigma_\pi & 0\\ 0 & \Sigma_K\end{pmatrix}\cdot\begin{pmatrix}F_\pi^{V*}\\ \sqrt{2}F_\pi^{V*}\end{pmatrix}\\ &= \frac{1}{24\pi}\Big(T_\pi\,\Sigma_\pi\,F_\pi^{V*}\,\theta\left(t-4M_\pi^2\right)\\ &\quad + 2T_K\,\Sigma_K\,F_K^{V*}\,\theta\left(t-4M_K^2\right)\Big).\end{aligned} \tag{34}$$

That becomes Eq. (4) after substituting the identity $q = \sqrt{t}\sigma/2$. Recalling that all the left-hand cut (LHC) part of T is included in K, then $T - K$ only contains the right-hand cut (RHC) and its unitarity relation is given by Eq. (33) for the two-channel assumption. One can also write [46]

$$\frac{1}{2i}\text{disc}\,\boldsymbol{\Omega}^{-1}(\mathbf{T}-\mathbf{K}) = -\left[\text{Im}\boldsymbol{\Omega}^{-1}\right]\mathbf{K}, \tag{35}$$

which leads to Eq. (13).

When $m_\Sigma^2 + m_\Lambda^2 - 2M_i^2 > 2m_{\text{exch}}^2$ and $\lambda(m_\Lambda^2, m_{\text{exch}}^2, M_i^2) < 0$ with $M_i = M_\pi$ (M_K) for the process $\Sigma\bar{\Lambda} \to \pi\pi$ ($\Sigma\bar{\Lambda} \to K\bar{K}$), the LHC and RHC will overlap, leading to the non-zero anomalous terms G_{anom} and $\mathbf{T}_{\text{anom}}$ in Eq. (4) and Eq. (13), respectively [24,38–41]. This indeed happens in the proton exchange diagram for the process $\Sigma\bar{\Lambda} \to K\bar{K}$. Such anomalous contributions are estimated by the dispersive integrals of the discontinuity along the cut that connects the anomalous threshold to the starting point of the RHC (the physical threshold of the two-body intermediate state). The anomalous threshold t_- is defined by [39]

$$\begin{aligned}t_- &= \frac{1}{2}(m_\Sigma^2 + m_\Lambda^2 + 2M_K^2 - m_N^2)\\ &\quad - \frac{1}{2m_N^2}\Big((m_\Sigma^2 - M_K^2)(m_\Lambda^2 - M_K^2)\\ &\quad + \lambda^{1/2}(m_\Sigma^2, m_N^2, M_K^2)\lambda^{1/2}(m_\Lambda^2, m_N^2, M_K^2)\Big).\end{aligned} \tag{36}$$

Numerically, $t_- = 0.935$ GeV located at the real axis of t just below the $K\bar{K}$ threshold. To go further, one first has to derive the discontinuity along the anomalous cut for the TFFs G and the scattering amplitudes $\mathbf{T}$. After implementing the partial-wave projection, namely the integration in Eq. (14) and Eq. (16), one obtains

$$K_N = \frac{f}{\kappa^3}\log\frac{Y+\kappa}{Y-\kappa} + \text{remainder}, \tag{37}$$

where

$$\begin{aligned}Y &= -(m_\Sigma^2 + m_\Lambda^2 + 2M_K^2 - t - 2m_N^2),\\ \kappa &= \lambda^{1/2}(t, m_\Sigma^2, m_\Lambda^2)\sigma_K(t).\end{aligned} \tag{38}$$

f is the coefficient of the logarithm which is a smooth function over the transferred momentum square t without any cut. The anomalous threshold is generated by the logarithm function. As illustrated in Refs. [24,39], the discontinuity of K_N along the anomalous cut reads

$$\frac{1}{2i}\text{disc}_{\text{anom}}\,K_N = \frac{f}{\kappa^2}\frac{2\pi}{(-\lambda(t, m_\Sigma^2, m_\Lambda^2))^{1/2}\sigma_K}. \tag{39}$$

Note that the argument of $\sqrt{z}$ is defined in the range of $[0, \pi)$ in the present work. Regarding $\mathbf{T}$, one can rewrite Eq. (35) into

$$\begin{aligned}\frac{1}{2i}\text{disc}_{\text{anom}}\,\boldsymbol{\Omega}^{-1}(\mathbf{T}-\mathbf{K}) &= -\left[\text{Im}\boldsymbol{\Omega}^{-1}\right]\frac{1}{2i}\text{disc}_{\text{anom}}\,\mathbf{K}\\ &= \left(\boldsymbol{\Omega}^{-1}\mathbf{t}_1^{1*}\boldsymbol{\Sigma}\right)\frac{1}{2i}\text{disc}_{\text{anom}}\,\mathbf{K},\end{aligned}$$

where we replace $(-\left[\text{Im}\boldsymbol{\Omega}^{-1}\right])$ with $(\boldsymbol{\Omega}^{-1}\mathbf{t}_1^{1*}\boldsymbol{\Sigma})$ in the second line since $\left[\text{Im}\Omega^{-1}\right]_{12} = \left[\text{Im}\Omega^{-1}\right]_{22} = 0$ below the $K\bar{K}$ threshold.[3] Finally, the discontinuity of the TFFs G along the anomalous cut can be read off straightforwardly in terms of that of $\mathbf{T}$,

$$\begin{aligned}\frac{1}{2i}\text{disc}_{\text{anom}}\,G &= \frac{1}{24\pi}\left((\mathbf{t}_1^{1*})^{-1}\frac{1}{2i}\text{disc}_{\text{anom}}\,(\mathbf{T}-\mathbf{K})\right)^T\mathbf{F}^{V*}\\ &= \frac{1}{24\pi}\left((\mathbf{t}_1^{1*})^{-1}\boldsymbol{\Omega}\left(\boldsymbol{\Omega}^{-1}\mathbf{t}_1^{1*}\boldsymbol{\Sigma}\right)\frac{1}{2i}\text{disc}_{\text{anom}}\,\mathbf{K}\right)^T\mathbf{F}^{V*}\\ &= \frac{1}{24\pi}\frac{1}{2i}(\text{disc}_{\text{anom}}\,\mathbf{K})^T\boldsymbol{\Sigma}\mathbf{F}^{V*}.\end{aligned} \tag{40}$$

[3] This replacement is necessary since $\left[\text{Im}\boldsymbol{\Omega}^{-1}\right]$ is solved numerically in our calculation and $\left[\text{Im}\Omega^{-1}\right]_{12} = \left[\text{Im}\Omega^{-1}\right]_{22} = 0$ always holds in the unphysical region. The combined quantity $\boldsymbol{\Omega}^{-1}\mathbf{t}_1^{1*}\boldsymbol{\Sigma}$ can be simplified analytically when multiplied to $\text{disc}_{\text{anom}}\,\mathbf{K}$. Then it turns out that the products $\boldsymbol{\Omega}^{-1}\mathbf{t}_1^{1*}$ and $\boldsymbol{\Sigma}\,\text{disc}_{\text{anom}}\,\mathbf{K}$, respectively, are finite along the anomalous cut. Moreover, the identity $-\left[\text{Im}\boldsymbol{\Omega}^{-1}\right] = \boldsymbol{\Omega}^{-1}\mathbf{t}_1^{1*}\boldsymbol{\Sigma}$ is checked numerically and does hold near the $K\bar{K}$ threshold.

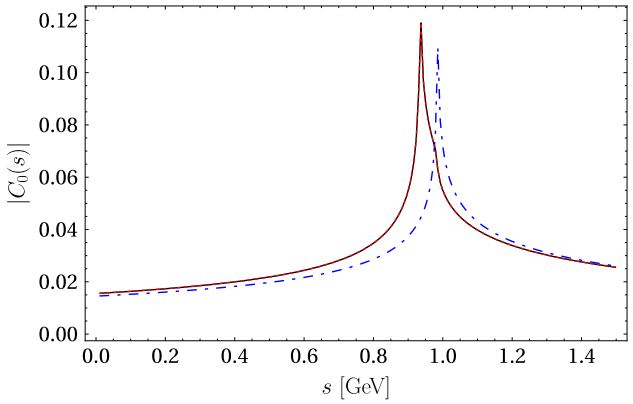

Fig. 10 The absolute values of the scalar triangle loop function $C_0(m_\Sigma^2, m_\Lambda^2, s, M_K^2, m_N^2, M_K^2)$ calculated numerically using Feynman parameters (solid black line) as well as dispersively with (dashed red line) and without the anomalous contribution (dot-dashed blue line). Note that the solid black and the dashed red line coincide

Substituting Eq. (39) into the above equation, one obtains

$$\frac{1}{2i}\text{disc}_{\text{anom}}\, G = \frac{1}{24}\frac{-f F_K^{V*} t}{(-\lambda(t, m_\Sigma^2, m_\Lambda^2))^{3/2}}. \tag{41}$$

Then we arrive at the expressions for G_{anom} and $\mathbf{T}_{\text{anom}}$. They are

$$G_{\text{anom}}(t) = \frac{t}{24\pi}\int_0^1 dx \frac{dt'(x)}{dx}\frac{1}{t'(x)-t} \times \frac{-f(t'(x))F_K^{V*}(t'(x))}{(-\lambda(t'(x), m_\Sigma^2, m_\Lambda^2))^{3/2}}, \tag{42}$$

$$\mathbf{T}_{\text{anom}}(t) = \boldsymbol{\Omega}(t)\frac{t}{\pi}\int_0^1 dx \frac{dt'(x)}{dx}\frac{1}{t'(x)-t} \times \frac{\left(\boldsymbol{\Omega}^{-1}\mathbf{t}_1^{1*}\boldsymbol{\Sigma}\right)\frac{1}{2i}\text{disc}_{\text{anom}}\,\mathbf{K}}{t'(t'-t-i\epsilon)}, \tag{43}$$

with $t'(x) = (1-x)\, t_- + x\, 4M_K^2$.

To cross-check whether this prescription is correct, we present the calculation of a scalar triangle loop function $C_0(m_\Sigma^2, m_\Lambda^2, s, M_K^2, m_N^2, M_K^2)$ in Fig. 10. The exact agreement is achieved only when the anomalous contribution is taken into account.

B The reduced amplitudes $K_{\pi/K}$ and $P_{0,\pi/K}$

The four-point amplitudes $\mathcal{M}_{\Sigma\bar{\Lambda}\to\pi\pi/K\bar{K}}(t,\theta)$ are calculated up to next-to leading order within the framework of SU(3) chiral perturbation theory. It turns out that the explicit inclusion of the decuplet baryon in the three-flavor ChPT Lagrangian is important to reproduce the correct $G_{E/M}(0)$ [4] and reasonable electric and magnetic transition radii, $\langle r_E^2\rangle$ and $\langle r_M^2\rangle$ [19]. We use the same Lagragians as in Ref. [19]. To be specific, the relevant interaction part of the leading order (LO) chiral Lagrangian that contains both the octet and decuplet states as active degrees of freedom for the reactions of interest is given by [21,58]

$$\mathcal{L}_{8+10}^{(1)} = \frac{D}{2}\langle\bar{B}\gamma^\mu\gamma_5\{u_\mu, B\}\rangle + \frac{F}{2}\langle\bar{B}\gamma^\mu\gamma_5[u_\mu, B]\rangle + \frac{1}{2\sqrt{2}}h_A\epsilon_{ade}g_{\mu\nu}\left(\bar{T}_{abc}^\mu u_{bd}^\nu B_{ce} + \bar{B}_{ec}u_{db}^\nu T_{abc}^\mu\right), \tag{44}$$

and the relevant NLO Lagrangian reads [59,60]

$$\mathcal{L}_8^{(2)} = \frac{i}{2}b_{10}\langle\bar{B}\{[u^\mu, u^\nu], \sigma_{\mu\nu}B\}\rangle, \tag{45}$$

where $\langle\cdots\rangle$ denotes a flavor trace. The chirally covariant derivatives are defined by

$$D^\mu B := \partial^\mu B + [\Gamma^\mu, B] \tag{46}$$

with

$$\Gamma_\mu = \frac{1}{2}\left(u^\dagger\left(\partial_\mu - i(v_\mu + a_\mu)\right)u + u\left(\partial_\mu - i(v_\mu - a_\mu)\right)u^\dagger\right). \tag{47}$$

Here, v and a are external sources and $u^2 = U = \exp(i\Phi/F_\Phi)$ with the Goldstone bosons encoded in the matrix

$$\Phi = \begin{pmatrix} \pi^0 + \frac{1}{\sqrt{3}}\eta & \sqrt{2}\,\pi^+ & \sqrt{2}\,K^+ \\ \sqrt{2}\,\pi^- & -\pi^0 + \frac{1}{\sqrt{3}}\eta & \sqrt{2}\,K^0 \\ \sqrt{2}\,K^- & \sqrt{2}\,\bar{K}^0 & -\frac{2}{\sqrt{3}}\eta \end{pmatrix}. \tag{48}$$

The octet baryons also make up a 3×3 matrix in the flavor space that is given by

$$B = \begin{pmatrix} \frac{1}{\sqrt{2}}\Sigma^0 + \frac{1}{\sqrt{6}}\Lambda & \Sigma^+ & p \\ \Sigma^- & -\frac{1}{\sqrt{2}}\Sigma^0 + \frac{1}{\sqrt{6}}\Lambda & n \\ \Xi^- & \Xi^0 & -\frac{2}{\sqrt{6}}\Lambda \end{pmatrix}. \tag{49}$$

Finally, T_{abc} is a totally symmetric flavor tensor that denotes the decuplet baryons,

$$T_{111} = \Delta^{++}, \quad T_{112} = \frac{1}{\sqrt{3}}\Delta^+,$$
$$T_{122} = \frac{1}{\sqrt{3}}\Delta^0, T_{222} = \Delta^-,$$

[4] Here, the normalization of electromagnetic Sigma-to-Lambda TFFs is estimated with the unsubtract dispersion relations, see Ref. [19] for more details.

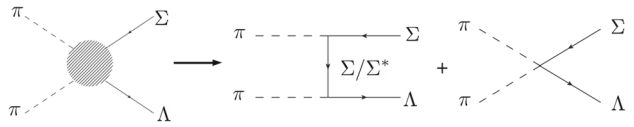

Fig. 11 Pictorial representation of the bare input of the four-point amplitude $\pi\pi \to \Sigma^0\bar{\Lambda}$ obtained up to NLO

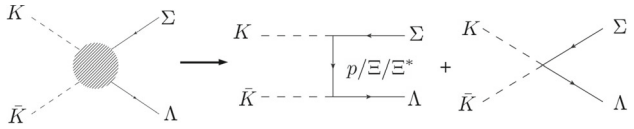

Fig. 12 Pictorial representation of the bare input of the four-point amplitude $K\bar{K} \to \Sigma^0\bar{\Lambda}$ obtained up to NLO

$$T_{113} = \frac{1}{\sqrt{3}}\,\Sigma^{*+}, \quad T_{123} = \frac{1}{\sqrt{6}}\,\Sigma^{*0}, \quad T_{223} = \frac{1}{\sqrt{3}}\,\Sigma^{*-},$$
$$T_{133} = \frac{1}{\sqrt{3}}\,\Xi^{*0}, \quad T_{233} = \frac{1}{\sqrt{3}}\,\Xi^{*-}, \quad T_{333} = \Omega. \tag{50}$$

The amplitudes $\mathcal{M}_{\Sigma\bar{\Lambda}\to\pi\pi/K\bar{K}}$ are described as a Born term in the LO plus a contact term in the NLO within the three-flavor ChPT, see Fig. 11 and Fig. 12.

From above Lagrangians, one obtains the Σ-exchange Born term for $\Sigma^0(p_1) + \bar{\Lambda}(p_2) \to \pi^-(p_3) + \pi^+(p_4)$,

$$\begin{aligned}
i\mathcal{M}_\Sigma &= i(\mathcal{M}_{\rm t} + \mathcal{M}_{\rm u})\\
i\mathcal{M}_{\rm t} &= \frac{DF}{\sqrt{3}F_\Phi^2}\left(\bar{v}_\Lambda\gamma^\mu\gamma_5 p_{3,\mu} S_{\Sigma^-,t}\gamma^\nu\gamma_5 p_{4,\nu} u_\Sigma\right),\\
i\mathcal{M}_{\rm u} &= \frac{-DF}{\sqrt{3}F_\Phi^2}\left(\bar{v}_\Lambda\gamma^\mu\gamma_5 p_{4,\mu} S_{\Sigma^+,u}\gamma^\nu\gamma_5 p_{3,\nu} u_\Sigma\right),
\end{aligned} \tag{51}$$

with $S_{\Sigma^-,t} = i((p_1-p_4)^\mu\gamma_\mu + m_\Sigma)/(t-m_\Sigma^2)$ and $S_{\Sigma^+,u} = i((p_1-p_3)^\mu\gamma_\mu + m_\Sigma)/(u-m_\Sigma^2)$ the propagator of the exchanged Σ in the t- and u-channel respectively. And the Σ^*-exchange Born term,

$$\begin{aligned}
i\mathcal{M}_{\Sigma^*} &= i(\mathcal{M}_{\rm t} + \mathcal{M}_{\rm u})\\
&= \left(\frac{-h_A}{2\sqrt{2}F_\Phi}\right)^2 \bar{v}_\Lambda g_{\mu\nu} p_3^\nu \Delta_t^{\mu\alpha}\left(\frac{-1}{\sqrt{3}}\right) g_{\alpha\beta} p_4^\beta u_\Sigma,\\
&\quad + \left(\frac{-h_A}{2\sqrt{2}F_\Phi}\right)^2 \bar{v}_\Lambda(-1) g_{\mu\nu} p_4^\nu \Delta_u^{\mu\alpha}\left(\frac{-1}{\sqrt{3}}\right) g_{\alpha\beta} p_3^\beta u_\Sigma,
\end{aligned} \tag{52}$$

with the spin-3/2 Rarita-Schwinger propagator [61]

$$\begin{aligned}
i\Delta^{\mu\nu}(p) = \frac{\gamma^\alpha p_\alpha + m}{p^2 - m^2}\Bigg(&g^{\mu\nu} - \frac{1}{3}\gamma^\mu\gamma^\nu\\
&- \frac{1}{3p^2}\gamma_\alpha\gamma_\beta p_\rho p_\lambda (g^{\mu\beta}g^{\nu\lambda}g^{\alpha\rho} + g^{\nu\alpha}g^{\mu\rho}g^{\beta\lambda})\Bigg)\\
&- \frac{2}{3m^2}\frac{p^\mu p^\nu}{p^2}(\gamma^\alpha p_\alpha + m)\\
&+ \frac{-i}{3\,m\,p^2}(g^{\mu\rho}g^{\nu\beta}g^{\alpha\lambda} + g^{\mu\alpha}g^{\nu\lambda}g^{\beta\rho})\sigma_{\alpha\beta}p_\rho p_\lambda,
\end{aligned}$$

and $t = (p_1 - p_4)^2$, $u = (p_1 - p_3)^2$. Here, m denotes the mass of the exchanged spin-3/2 resonance. The NLO contact term for the reaction $\Sigma^0(p_1) + \bar{\Lambda}(p_2) \to \pi^-(p_3) + \pi^+(p_4)$ is given by

$$\begin{aligned}
\mathcal{M}_{\rm NLO} = &\left(b_{10}\frac{1}{F_\Phi^2}\frac{4}{\sqrt{3}}\right)\frac{1}{2}\\
&\times\Bigg((m_\Sigma + m_\Lambda)\left(-\bar{v}_\Lambda\gamma^\mu(p_4 - p_3)_\mu u_\Sigma\right)\\
&+ (u-t)\bar{v}_\Lambda u_\Sigma\Bigg).
\end{aligned} \tag{53}$$

The corresponding expressions for the $\Sigma^0(p_1) + \bar{\Lambda}(p_2) \to K^-(p_3) + K^+(p_4)$ ($\mathcal{M}_{\Sigma^0\bar{\Lambda}\to K^0\bar{K}^0} = -\mathcal{M}_{\Sigma^0\bar{\Lambda}\to K^+K^-}$ in the isospin limit) read

$$\begin{aligned}
i\mathcal{M}_{\rm born} &= i(\mathcal{M}_{\rm u} + \mathcal{M}_{\rm t} + \mathcal{M}_{\Xi^*}),\\
i\mathcal{M}_{\rm u} &= \frac{1}{F_\Phi^2}\left(\frac{-D}{2\sqrt{3}} + \frac{-\sqrt{3}F}{2}\right)\frac{D-F}{2}\\
&\quad\times\left(\bar{v}_\Lambda\gamma^\mu\gamma_5 p_{4,\mu} S_{p,u}\gamma^\nu\gamma_5 p_{3,\nu} u_\Sigma\right),\\
i\mathcal{M}_{\rm t} &= \frac{1}{F_\Phi^2}\left(\frac{-D}{2\sqrt{3}} + \frac{\sqrt{3}F}{2}\right)\frac{D+F}{2}\\
&\quad\times\left(\bar{v}_\Lambda\gamma^\mu\gamma_5 p_{3,\mu} S_{\Xi,t}\gamma^\nu\gamma_5 p_{4,\nu} u_\Sigma\right),\\
i\mathcal{M}_{\Xi^*} &= \left(\frac{-h_A}{2\sqrt{2}F_\Phi}\right)^2 \bar{v}_\Lambda(+1) g_{\mu\nu} p_3^\nu \Delta_t^{\mu\alpha}\left(\frac{-1}{\sqrt{3}}\right) g_{\alpha\beta} p_4^\beta u_\Sigma,\\
\mathcal{M}_{\rm NLO} &= \left(b_{10}\frac{1}{F_\Phi^2}\frac{2}{\sqrt{3}}\right)\frac{1}{2}\\
&\quad\times\left((m_\Sigma + m_\Lambda)\left(-\bar{v}_\Lambda\gamma^\mu(p_4 - p_3)_\mu u_\Sigma\right) + (u-t)\bar{v}_\Lambda u_\Sigma\right),
\end{aligned} \tag{54}$$

with $S_{p,u} = i((p_1 - p_3)^\mu\gamma_\mu + m_p)/(u - m_p^2)$ and $S_{\Xi,t} = i((p_1 - p_4)^\mu\gamma_\mu + m_\Xi)/(t - m_\Xi^2)$ the propagator of the exchanged proton and Ξ baryon, respectively. To proceed, it is helpful to introduce the following equivalents,

$$\begin{aligned}
E1 &\equiv \frac{\bar{v}_{1/2,\Lambda}\gamma^\mu(p_1 - p_2)_\mu u_{1/2,\Sigma}}{\bar{v}_{1/2,\Lambda}\gamma^3 u_{1/2,\Sigma}} = \frac{\bar{v}_{1/2,\Lambda}u_{1/2,\Sigma}(m_\Lambda + m_\Sigma)}{\bar{v}_{1/2,\Lambda}\gamma^3 u_{1/2,\Sigma}}\\
&= \frac{(m_\Sigma + m_\Lambda)^2 - s}{2p_z},\\
E2 &\equiv \frac{\bar{v}_{1/2,\Lambda}\gamma^\mu(p_4 - p_3)_\mu u_{1/2,\Sigma}}{\bar{v}_{1/2,\Lambda}\gamma^3 u_{1/2,\Sigma}} = -2p_{\rm c.m.}\cos\theta,\\
M1 &\equiv \frac{\bar{v}_{-1/2,\Lambda}u_{1/2,\Sigma}(m_\Lambda + m_\Sigma)}{\bar{v}_{-1/2,\Lambda}\gamma^1 u_{1/2,\Sigma}} = 0,\\
M2 &\equiv \frac{\bar{v}_{-1/2,\Lambda}\gamma^\mu(p_4 - p_3)_\mu u_{1/2,\Sigma}}{\bar{v}_{-1/2,\Lambda}\gamma^1 u_{1/2,\Sigma}} = -2p_{\rm c.m.}\sin\theta,
\end{aligned} \tag{55}$$

where $s = (p_1 + p_2)^2 = (p_3 + p_4)^2$ is the center-of-mass energy. p_z and $p_{\rm c.m.}$ denote the modulus of the three-dimensional center-of-mass momenta of the $\Sigma\bar{\Lambda}$ and $\pi\pi/K\bar{K}$ two-body systems, respectively, i.e. $p_{\rm c.m.} = q_{\pi/K}$. The equations (55) are calculated in the center-of-mass frame with the p_z the modulus of the three-momentum along the direction of the z-axis and θ is the scattering angle of π or K. Substitute Eqs. (51), (52), (53), (54) into Eqs. (14),(15),(16), (17), we obtain $P^E_{0,\pi}$, $P^M_{0,\pi}$, K^E_π and K^M_π for the $\pi\pi$ inelasticity,

$$
\begin{aligned}
P^E_{0,\pi} &= P^E_\Sigma + P^E_{\Sigma^*}\,, \qquad (56)\\
P^E_\Sigma &= \frac{3}{2}\int_0^\pi d\theta \sin\theta\, \cos\theta \frac{DF}{\sqrt{3}F_\Phi^2}\frac{E2}{p_{\rm c.m.}} = -\frac{2}{\sqrt{3}}\frac{DF}{F_\Phi^2}\,,\\
P^E_{\Sigma^*} &= \frac{3}{2}\int_0^\pi d\theta \sin\theta\, \cos\theta \left(\frac{-h_A}{2\sqrt{2}F_\pi}\right)^2 \frac{1}{\sqrt{3}}\Bigg(\frac{t-u}{12m^2_{\Sigma^*}}\frac{E1}{p_{\rm c.m.}}\\
&\quad + \frac{E2}{p_{\rm c.m.}}\frac{1}{12m^2_{\Sigma^*}}(-2m^2_{\Sigma^*} - 2m_{\Sigma^*}(m_\Sigma + m_\Lambda) + m^2_\Sigma\\
&\quad + m^2_\Lambda + s - 6M^2_\pi)\Bigg)\\
&= \frac{h_A^2}{24\sqrt{3}F_\Phi^2}\frac{(m_\Lambda + m_{\Sigma^*})(m_\Sigma + m_{\Sigma^*})}{m^2_{\Sigma^*}} + \mathcal{O}(M_\pi^2, s)\,.\\
K^E_\pi &= K^E_\Sigma + K^E_{\Sigma^*}\,,\\
K^E_\Sigma &= \frac{3}{2}\int_0^\pi d\theta \sin\theta\, \cos\theta \frac{DF}{\sqrt{3}F_\Phi^2}\\
&\quad \times\Bigg(\frac{E1}{p_{\rm c.m.}} m_\Sigma\,(m_\Sigma - m_\Lambda)\left(\frac{1}{t-m^2_\Sigma} - \frac{1}{u-m^2_\Sigma}\right)\\
&\quad + \frac{E2}{p_{\rm c.m.}} m_\Sigma\,(m_\Sigma + m_\Lambda)\left(\frac{1}{t-m^2_\Sigma} + \frac{1}{u-m^2_\Sigma}\right)\Bigg)\,,\\
K^E_{\Sigma^*} &= \frac{3}{2}\int_0^\pi d\theta \sin\theta\, \cos\theta \left(\frac{-h_A}{2\sqrt{2}F_\pi}\right)^2 \frac{1}{\sqrt{3}}\\
&\quad \times\Bigg(+\frac{F(s)}{m_\Sigma + m_\Lambda}\frac{E1}{p_{\rm c.m.}}\left(\frac{1}{u-m^2_{\Sigma^*}} - \frac{1}{t-m^2_{\Sigma^*}}\right)\\
&\quad + \frac{E2}{p_{\rm c.m.}}\left(\frac{1}{u-m^2_{\Sigma^*}} + \frac{1}{t-m^2_{\Sigma^*}}\right)\frac{G(s)}{2}\Bigg)\,, \qquad (57)
\end{aligned}
$$

where

$$
\begin{aligned}
F(s) &= \left(\frac{m_\Sigma + m_\Lambda}{2} + m_{\Sigma^*}\right)H_1(s)\\
&\quad + \left(\frac{m_\Sigma + m_\Lambda}{2} - m_{\Sigma^*}\right)H_2\,,\\
G(s) &= H_1(s) + H_2\,,\\
H_1(s) &= \frac{m^2_\Sigma + m^2_\Lambda - s}{2}\\
&\quad - \frac{(m^2_\Lambda + m^2_{\Sigma^*} - M^2_\pi)(m^2_\Sigma + m^2_{\Sigma^*} - M^2_\pi)}{4m^2_{\Sigma^*}}\,,\\
H_2 &= \frac{1}{3}\left(m_\Lambda + \frac{m^2_\Lambda + m^2_{\Sigma^*} - M^2_\pi}{2m_{\Sigma^*}}\right)\\
&\quad \times\left(m_\Sigma + \frac{m^2_\Sigma + m^2_{\Sigma^*} - M^2_\pi}{2m_{\Sigma^*}}\right)\,.\\
P^M_{0,\pi} &= P^M_\Sigma + P^M_{\rm NLO} - K^M_{\Sigma^*,\rm low}\,,\\
P^M_\Sigma &= \frac{3}{4}\int_0^\pi d\theta \sin\theta\, \sin\theta \frac{DF}{\sqrt{3}F_\Phi^2}\frac{M2}{p_{\rm c.m.}} = -\frac{2}{\sqrt{3}}\frac{DF}{F_\Phi^2}\,,\\
P^M_{\rm NLO} &= \frac{3}{4}\int_0^\pi d\theta \sin\theta\, \sin\theta \left(b_{10}\frac{1}{F_\Phi^2}\frac{4}{\sqrt{3}}\right)\frac{(m_\Sigma + m_\Lambda)}{2}\frac{-M2}{p_{\rm c.m.}}\\
&= \frac{4}{\sqrt{3}}\frac{b_{10}}{F_\Phi^2}(m_\Lambda + m_\Sigma)\,. \qquad (58)\\
K^M_\pi &= K^M_\Sigma + K^M_{\Sigma^*}\,,\\
K^M_\Sigma &= \frac{3}{4}\int_0^\pi d\theta \sin\theta\, \sin\theta \frac{DF}{\sqrt{3}F_\Phi^2}\frac{M2}{p_{\rm c.m.}}\\
&\quad \times m_\Sigma\,(m_\Sigma + m_\Lambda)\left(\frac{1}{t-m^2_\Sigma} + \frac{1}{u-m^2_\Sigma}\right)\,,\\
K^M_{\Sigma^*} &= \frac{3}{4}\int_0^\pi d\theta \sin\theta\, \sin\theta \left(\frac{-h_A}{2\sqrt{2}F_\pi}\right)^2 \frac{1}{\sqrt{3}}\\
&\quad \times\left(+\frac{M2}{p_{\rm c.m.}}\left(\frac{1}{u-m^2_{\Sigma^*}} + \frac{1}{t-m^2_{\Sigma^*}}\right)\frac{G(s)}{2}\right)\,. \qquad (59)
\end{aligned}
$$

Note that we subtract a term $K^M_{\Sigma^*,\rm low}$ in the polynomial part of the magnetic amplitude $P^M_{0,\pi}$, which denotes the low-energy limit of the LHC contribution of the decuplet-exchanged magnetic amplitude. It is proposed to remove the doubly counted decuplet baryon contribution caused by the using of the resonance saturation assumption for the estimation of b_{10} in the present ChPT framework. A similar term $K^E_{\Sigma^*,\rm low}$ should be subtracted in $P^E_{0,\pi}$. However, it belongs to a higher chiral order and is dropped here. Note that $P^E_{\rm NLO}$ belongs to $P_1(s)$ that is beyond the accuracy of Eq. (13) and is also dropped. Taking the same convention with Ref. [19], $K^M_{\Sigma^*,\rm low}$ is given by

$$
\begin{aligned}
K^M_{\Sigma^*,\rm low} &= \lim_{s\to 0}\lim_{m_\Lambda\to m_\Sigma}\lim_{M_\pi\to 0} K^M_{\Sigma^*}(s)\\
&= \frac{h_A^2}{24\sqrt{3}F_\Phi^2}\frac{(-m^2_{\Sigma^*} + 4m_{\Sigma^*}m_\Sigma - m^2_\Sigma)\,(m_{\Sigma^*} + m_\Sigma)}{m^2_{\Sigma^*}\,(m_{\Sigma^*} - m_\Sigma)}\,.
\end{aligned}
$$

And similarly, the $P^E_{0,K}$, $P^M_{0,K}$, K^E_K and K^M_K for the $K\bar{K}$ inelasticity read

$$P^E_{0,K} = P^E_{\rm born} + P^E_{\Xi^*}, \tag{60}$$

with

$$\begin{aligned}
P^E_{\rm born} &= \frac{3}{2}\int_0^\pi d\theta \sin\theta\,\cos\theta\Big(\frac{1}{2}\Big(g_A(m_\Lambda+m_\Sigma+2m_N)\\
&\quad + g_B(m_\Lambda+m_\Sigma+2m_\Xi)\Big)\frac{E1}{(m_\Lambda+m_\Sigma)p_{\rm c.m.}}\\
&\quad + \frac{g_B-g_A}{2}\frac{E2}{p_{\rm c.m.}}\Big)\\
&= g_A - g_B\,,\\
P^E_{\Xi^*} &= \frac{3}{2}\int_0^\pi d\theta \sin\theta\,\cos\theta\frac{h_A^2}{8\sqrt{3}F_\Phi^2}\Big(\Big(\frac{1}{12m^2_{\Xi^*}}\\
&\quad\times(m_\Lambda+m_\Sigma)(t-m^2_{\Xi^*}) + \frac{1}{12m^2_{\Xi^*}}(m_\Lambda+m_\Sigma+2m_{\Xi^*})\\
&\quad\times(-m_\Lambda^2-m_\Sigma^2+2M_K^2+2m^2_{\Xi^*}\\
&\quad + m_{\Xi^*}(m_\Lambda+m_\Sigma))\Big)\frac{E1}{(m_\Lambda+m_\Sigma)p_{\rm c.m.}}\\
&\quad + \Big(\frac{1}{12}(1-\frac{t}{m^2_{\Xi^*}}) + \frac{1}{12m^2_{\Xi^*}}(m_\Lambda^2+m_\Sigma^2-2M_K^2\\
&\quad - 2m^2_{\Xi^*} - m_{\Xi^*}(m_\Lambda+m_\Sigma))\Big)\frac{E2}{p_{\rm c.m.}}\Big)\\
&= \frac{h_A^2(m_\Lambda+m_{\Xi^*})(m_\Sigma+m_{\Xi^*})}{48\sqrt{3}F_\Phi^2 m^2_{\Xi^*}} + \mathcal{O}(s,M_K^2)\,.\\
K^E_K &= K^E_N + K^E_\Xi + K^E_{\Xi^*}\,,\\
K^E_N &= \frac{3}{2}\int_0^\pi d\theta \sin\theta\,\cos\theta\Big(\frac{E1}{(m_\Lambda+m_\Sigma)p_{\rm c.m.}}\\
&\quad\times g_A\frac{(m_\Lambda+m_N)(m_\Sigma+m_N)(m_\Lambda+m_\Sigma-2m_N)}{2(m_N^2-u)}\\
&\quad + \frac{E2}{p_{\rm c.m.}}\frac{1}{2}\frac{g_A(m_\Lambda+m_N)(m_\Sigma+m_N)}{m_N^2-u}\Big)\,,\\
K^E_\Xi &= \frac{3}{2}\int_0^\pi d\theta \sin\theta\,\cos\theta\Big(\frac{E1}{(m_\Lambda+m_\Sigma)p_{\rm c.m.}}\\
&\quad\times g_B\frac{(m_\Lambda+m_\Xi)(m_\Sigma+m_\Xi)(m_\Lambda+m_\Sigma-2m_\Xi)}{2(m_\Xi^2-t)}\\
&\quad + \frac{E2}{p_{\rm c.m.}}\frac{1}{2}\Big(-\frac{g_B(m_\Lambda+m_\Xi)(m_\Sigma+m_\Xi)}{m_\Xi^2-t}\Big)\Big)\,,\\
K^E_{\Xi^*} &= \frac{3}{2}\int_0^\pi d\theta \sin\theta\,\cos\theta\frac{h_A^2}{8\sqrt{3}F_\Phi^2}\Big(\frac{-\tilde{F}(s)}{12m^2_{\Xi^*}(m^2_{\Xi^*}-t)}\\
&\quad\times\frac{E1}{(m_\Lambda+m_\Sigma)p_{\rm c.m.}} + \frac{E2}{p_{\rm c.m.}}\frac{1}{12m^2_{\Xi^*}(m^2_{\Xi^*}-t)}\tilde{G}(s)\Big)\,,
\end{aligned}\tag{61}$$

where

$$\begin{aligned}
\tilde{F}(s) &= -M_K^4(m_\Lambda+m_\Sigma+4m_{\Xi^*})\\
&\quad + M_K^2(m_\Lambda^3+8m^3_{\Xi^*}+4m^2_{\Xi^*}m_\Sigma+3m_{\Xi^*}m_\Sigma^2+m_\Sigma^3\\
&\quad + m_\Lambda^2(3m_{\Xi^*}+m_\Sigma)+m_\Lambda(4m^2_{\Xi^*}-2m_{\Xi^*}m_\Sigma+m_\Sigma^2))\\
&\quad + (m_\Lambda+m_{\Xi^*})(m_\Sigma+m_{\Xi^*})(m_\Lambda^2(2m_{\Xi^*}-m_\Sigma)\\
&\quad + m_\Lambda(m^2_{\Xi^*}-m_\Sigma^2)+m_{\Xi^*}(-4m^2_{\Xi^*}+2m_\Sigma^2+m_{\Xi^*}m_\Sigma))\\
&\quad - 3m^2_{\Xi^*}(m_\Lambda+2m_{\Xi^*}+m_\Sigma)s\,,\\
\tilde{G}(s) &= 3m^2_{\Xi^*}s + M_K^4 + (m_\Lambda+m_{\Xi^*})(m_\Sigma+m_{\Xi^*})\\
&\quad\times(m_{\Xi^*}(m_{\Xi^*}-2m_\Sigma)+m_\Lambda(-2m_{\Xi^*}+m_\Sigma))\\
&\quad - M_K^2(m_\Lambda^2+m_\Sigma^2+2m^2_{\Xi^*}-m_{\Xi^*}(m_\Lambda+m_\Sigma))\,.
\end{aligned}$$

Note that the Pascalutsa prescription of the spin-3/2 particle will bring an ambiguity in the $P^E_{\Sigma^*}$ and $P^E_{\Xi^*}$ while it keeps $K^E_{\Sigma^*}$ and $K^E_{\Xi^*}$ consistent with the interaction between the decuplet and octet states listed in Eq. (44), see Ref. [19] for the details. The uncertainties on the TFFs originating from such ambiguity, however, are negligible when compared with the parameter errors. And we take he same convention with Ref. [19] where the $\mathcal{O}(M_\pi^2,s)$ and $\mathcal{O}(M_K^2,s)$ terms are dropped in the $P^E_{\Sigma^*}$ and $P^E_{\Xi^*}$. Further,

$$\begin{aligned}
P^M_{0,K} &= P^M_{\rm born} + P^M_{\rm NLO} - K^M_{\Xi^*,\rm low}\,,\\
P^M_{\rm born} &= \frac{3}{4}\int_0^\pi d\theta \sin\theta\,\sin\theta\frac{g_B-g_A}{2}\frac{M2}{p_{\rm c.m.}} = g_A - g_B\,,\\
P^M_{\rm NLO} &= \frac{3}{4}\int_0^\pi d\theta \sin\theta\,\sin\theta\Big(b_{10}\frac{1}{F_\Phi^2}\frac{2}{\sqrt{3}}\Big)\frac{(m_\Sigma+m_\Lambda)}{2}\frac{-M2}{p_{\rm c.m.}}\\
&= \frac{2}{\sqrt{3}}\frac{b_{10}}{F_\Phi^2}(m_\Lambda+m_\Sigma)\,.\\
K^M_K &= K^M_N + K^M_\Xi + K^M_{\Xi^*}\,,\\
K^M_N &= \frac{3}{4}\int_0^\pi d\theta \sin\theta\,\sin\theta\Big(-\frac{M2}{p_{\rm c.m.}}\frac{1}{2}\\
&\quad\times\Big(\frac{g_A(m_\Lambda+m_N)(m_\Sigma+m_N)}{u-m_N^2}\Big)\Big)\,,\\
K^M_\Xi &= \frac{3}{4}\int_0^\pi d\theta \sin\theta\,\sin\theta\Big(-\frac{M2}{p_{\rm c.m.}}\frac{1}{2}\\
&\quad\times\Big(-\frac{g_B(m_\Lambda+m_\Xi)(m_\Sigma+m_\Xi)}{t-m_\Xi^2}\Big)\Big)\,,\\
K^M_{\Xi^*} &= \frac{3}{4}\int_0^\pi d\theta \sin\theta\,\sin\theta\frac{h_A^2}{8\sqrt{3}F_\Phi^2}\\
&\quad\times\Big(+\frac{M2}{p_{\rm c.m.}}\frac{1}{12m^2_{\Xi^*}(m^2_{\Xi^*}-t)}\tilde{G}(s)\Big)\,.\\
K^M_{\Xi^*,\rm low} &= \lim_{s\to0}\lim_{m_\Lambda\to m_\Sigma}\lim_{M_K\to0}K^M_{\Xi^*}(s)
\end{aligned}\tag{62}$$

$$= \frac{h_A^2}{48\sqrt{3}F_\Phi^2} \frac{(-m_{\Xi^*}^2 + 4m_{\Xi^*}m_\Sigma - m_\Sigma^2)(m_{\Xi^*} + m_\Sigma)}{m_{\Sigma^*}^2 (m_{\Xi^*} - m_\Sigma)}. \tag{63}$$

Here, g_A and g_B are defined as

$$g_A = \frac{1}{F_\Phi^2}\left(\frac{-D}{2\sqrt{3}} + \frac{-\sqrt{3}F}{2}\right)\frac{D-F}{2},$$
$$g_B = \frac{1}{F_\Phi^2}\left(\frac{-D}{2\sqrt{3}} + \frac{\sqrt{3}F}{2}\right)\frac{D+F}{2}.$$

There are only three different kinds of integration over angle involved in the $K^{E/M}$. Expanding u and t in the center-of-mass frame, one has

$$t(s,\theta) = -\frac{1}{2}Y(s) + \frac{1}{2}\kappa(s)\cos\theta,$$
$$u(s,\theta) = -\frac{1}{2}Y(s) - \frac{1}{2}\kappa(s)\cos\theta,$$

with $Y(s)$ and $\kappa(s)$ given by Eq. (38). Then three different integrals are expressed as

$$A = \int_0^\pi d\theta \frac{\sin\theta\cos\theta}{t - m_{\text{exch}}^2}\frac{E1}{p_{\text{c.m.}}} \propto \int_0^\pi d\theta \frac{\cos\theta\sin\theta}{t - m_{\text{exch}}^2}\frac{1}{p_{\text{c.m.}}}$$
$$= \frac{4}{\kappa(s)^2} - \frac{2Y(s)}{\kappa(s)^2}\tilde{K}(s),$$
$$B = \int_0^\pi d\theta \frac{\sin\theta\cos\theta}{t - m_{\text{exch}}^2}\frac{E2}{p_{\text{c.m.}}} \propto \int_0^\pi d\theta \frac{\cos^2\theta\sin\theta}{t - m_{\text{exch}}^2}$$
$$= \frac{4Y(s)}{\kappa(s)^2} - \frac{2Y(s)^2}{\kappa(s)^2}\tilde{K}(s),$$
$$C = \int_0^\pi d\theta \frac{\sin\theta\sin\theta}{t - m_{\text{exch}}^2}\frac{M2}{p_{\text{c.m.}}} \propto \int_0^\pi d\theta \frac{\sin^2\theta\sin\theta}{t - m_{\text{exch}}^2}$$
$$= \frac{-2Y(s)}{\kappa(s)^2} + \frac{Y(s)^2 - \kappa(s)^2}{\kappa(s)^2}\tilde{K}(s).$$

For the u cases, there is an extra sign in A. Here we dropped all irrelevant coefficients of θ-dependent terms. m_{exch} denotes the mass of exchanged particle, while $\tilde{K}(s)$ is defined as [24]

$$\tilde{K}(s) = \begin{cases} \frac{1}{\kappa(s)}\log\frac{Y(s)+\kappa(s)}{Y(s)-\kappa(s)}, & (m_\Sigma + m_\Lambda)^2 \le s, \\ \frac{2}{|\kappa(s)|}(\arctan\frac{|\kappa(s)|}{Y(s)}), & s_0 \le s \le (m_\Sigma + m_\Lambda)^2, \\ \frac{2}{|\kappa(s)|}(\arctan\frac{|\kappa(s)|}{Y(s)} + \pi), & 4M_\pi^2 \le s \le s_0, \end{cases}$$

with $s_0 = m_\Sigma^2 + m_\Lambda^2 + 2M_\pi^2 - 2m_{\text{exch}}^2$. Finally, M_π is replaced by M_K when calculating the expressions for the $K\bar{K}$ channel.

References

1. R. Pohl et al., The size of the proton. Nature **466**, 213–216 (2010). https://doi.org/10.1038/nature09250
2. A. Denig, G. Salme, Nucleon electromagnetic form factors in the timelike region. Prog. Part. Nucl. Phys. **68**, 113–157 (2013). https://doi.org/10.1016/j.ppnp.2012.09.005. arXiv:1210.4689
3. S. Pacetti, R. Baldini Ferroli, E. Tomasi-Gustafsson, Proton electromagnetic form factors: basic notions, present achievements and future perspectives. Phys. Rept. **550–551**, 1–103 (2015). https://doi.org/10.1016/j.physrep.2014.09.005
4. V. Punjabi, C.F. Perdrisat, M.K. Jones, E.J. Brash, C.E. Carlson, The structure of the nucleon: elastic electromagnetic form factors. Eur. Phys. J. A **51**, 79 (2015). https://doi.org/10.1140/epja/i2015-15079-x. arXiv:1503.01452
5. C. Peset, A. Pineda, O. Tomalak, The proton radius (puzzle?) and its relatives. Prog. Part. Nucl. Phys. **121**, 103901 (2021). https://doi.org/10.1016/j.ppnp.2021.103901. arXiv:2106.00695
6. H. Gao, M. Vanderhaeghen, The proton charge radius. Rev. Mod. Phys. **94**(1), 015002 (2022). https://doi.org/10.1103/RevModPhys.94.015002. arXiv:2105.00571
7. I.T. Lorenz, H.-W. Hammer, U.-G. Meißner, The size of the proton—closing in on the radius puzzle. Eur. Phys. J. A **48**, 151 (2012). https://doi.org/10.1140/epja/i2012-12151-1. arXiv:1205.6628
8. I.T. Lorenz, U.-G. Meißner, H.-W. Hammer, Y.-B. Dong, Theoretical constraints and systematic effects in the determination of the proton form factors. Phys. Rev. D **91**(1), 014023 (2015). https://doi.org/10.1103/PhysRevD.91.014023. arXiv:1411.1704
9. M. Hoferichter, B. Kubis, J. Ruiz de Elvira, H.-W. Hammer, U.-G. Meißner, On the $\pi\pi$ continuum in the nucleon form factors and the proton radius puzzle. Eur. Phys. J. A **52**(11), 331 (2016). https://doi.org/10.1140/epja/i2016-16331-7. arXiv:1609.06722
10. Y.-H. Lin, H.-W. Hammer, U.-G. Meißner, High-precision determination of the electric and magnetic radius of the proton. Phys. Lett. B **816**, 136254 (2021). https://doi.org/10.1016/j.physletb.2021.136254. arXiv:2102.11642
11. G.F. Chew, R. Karplus, S. Gasiorowicz, F. Zachariasen, Electromagnetic structure of the nucleon in local-field theory. Phys. Rev. **110**(1), 265 (1958). https://doi.org/10.1103/PhysRev.110.265
12. P. Federbush, M.L. Goldberger, S.B. Treiman, Electromagnetic structure of the nucleon. Phys. Rev. **112**, 642–665 (1958). https://doi.org/10.1103/PhysRev.112.642
13. G. Höhler, E. Pietarinen, I. Sabba-Stefanescu, F. Borkowski, G.G. Simon, V.H. Walther, R.D. Wendling, Analysis of electromagnetic nucleon form-factors. Nucl. Phys. B **114**, 505–534 (1976). https://doi.org/10.1016/0550-3213(76)90449-1
14. P. Mergell, U.-G. Meißner, D. Drechsel, Dispersion theoretical analysis of the nucleon electromagnetic form-factors. Nucl. Phys. A **596**, 367–396 (1996). https://doi.org/10.1016/0375-9474(95)00339-8. arXiv:hep-ph/9506375
15. M.A. Belushkin, H.-W. Hammer, U.-G. Meißner, Dispersion analysis of the nucleon form-factors including meson continua. Phys. Rev. C **75**, 035202 (2007). https://doi.org/10.1103/PhysRevC.75.035202. arXiv:hep-ph/0608337
16. G.P. Lepage, S.J. Brodsky, Exclusive processes in perturbative quantum chromodynamics. Phys. Rev. D **22**, 2157 (1980). https://doi.org/10.1103/PhysRevD.22.2157
17. Y.-H. Lin, H.-W. Hammer, U.-G. Meißner, Dispersion-theoretical analysis of the electromagnetic form factors of the nucleon: past, present and future. Eur. Phys. J. A **57**, 255 (2021). https://doi.org/10.1140/epja/s10050-021-00562-0. arXiv:2106.06357
18. Y.-H. Lin, H.-W. Hammer, U.-G. Meißner, New insights into the Nucleon's electromagnetic structure. Phys. Rev. Lett. **128**(5),

052002 (2022). https://doi.org/10.1103/PhysRevLett.128.052002. arXiv:2109.12961
19. C. Granados, S. Leupold, E. Perotti, The electromagnetic Sigma-to-Lambda hyperon transition form factors at low energies. Eur. Phys. J. A **53**(6), 117 (2017). https://doi.org/10.1140/epja/i2017-12324-4. arXiv:1701.09130
20. V. Pascalutsa, M. Vanderhaeghen, S.N. Yang, Electromagnetic excitation of the Delta(1232)-resonance. Phys. Rept. **437**, 125–232 (2007). https://doi.org/10.1016/j.physrep.2006.09.006. arXiv:hep-ph/0609004
21. B. Kubis, U.-G. Meißner, Baryon form-factors in chiral perturbation theory. Eur. Phys. J. C **18**, 747–756 (2001). https://doi.org/10.1007/s100520100570. arXiv:hep-ph/0010283
22. J. Haidenbauer, U.-G. Meißner, The electromagnetic form factors of the Λ in the timelike region. Phys. Lett. B **761**, 456–461 (2016). https://doi.org/10.1016/j.physletb.2016.08.067. arXiv:1608.02766
23. J.M. Alarcón, A.N. Hille Blin, M.J. Vicente Vacas, C. Weiss, Peripheral transverse densities of the baryon octet from chiral effective field theory and dispersion analysis. Nucl. Phys. A **964**, 18–54 (2017). https://doi.org/10.1016/j.nuclphysa.2017.05.002. arXiv:1703.04534
24. O. Junker, S. Leupold, E. Perotti, T. Vitos, Electromagnetic form factors of the transition from the spin-3/2 Σ to the Λ hyperon. Phys. Rev. C **101**(1), 015206 (2020). https://doi.org/10.1103/PhysRevC.101.015206. arXiv:1910.07396
25. J. Haidenbauer, U.-G. Meißner, L.-Y. Dai, Hyperon electromagnetic form factors in the timelike region. Phys. Rev. D **103**(1), 014028 (2021). https://doi.org/10.1103/PhysRevD.103.014028. arXiv:2011.06857
26. M. Irshad, D. Liu, X. Zhou, G. Huang, Electromagnetic form factors of Σ hyperons. Symmetry **14**(1), 69 (2022). https://doi.org/10.3390/sym14010069
27. R. García-Martín, R. Kamiński, J. R. Peláez, J. Ruiz de Elvira, F. J. Ynduráin, The Pion-pion scattering amplitude. IV: Improved analysis with once subtracted Roy-like equations up to 1100 MeV, Phys. Rev. D **83**, 074004 (2011). https://doi.org/10.1103/PhysRevD.83.074004 arXiv:1102.2183
28. C. Hanhart, A new parameterization for the pion vector form factor. Phys. Lett. B **715**, 170–177 (2012). https://doi.org/10.1016/j.physletb.2012.07.038. arXiv:1203.6839
29. J. Bijnens, T. Husek, Six-pion amplitude. Phys. Rev. D **104**(5), 054046 (2021). https://doi.org/10.1103/PhysRevD.104.054046. arXiv:2107.06291
30. J. Gasser, U.-G. Meißner, Chiral expansion of pion form factors beyond one loop. Nucl. Phys. B **357**, 90–128 (1991). https://doi.org/10.1016/0550-3213(91)90460-F
31. B. Moussallam, N(f) dependence of the quark condensate from a chiral sum rule. Eur. Phys. J. C **14**, 111–122 (2000). https://doi.org/10.1007/s100520050738. arXiv:hep-ph/9909292
32. A. Adamo et al., New results on meson spectroscopy from Obelix. Nucl. Phys. A **558**, 13C-26C (1993). https://doi.org/10.1016/0375-9474(93)90379-C
33. C. Amsler et al., Observation of a scalar resonance decaying to pi+ pi- pi0 pi0 in anti-p p annihilation at rest. Phys. Lett. B **322**, 431–440 (1994). https://doi.org/10.1016/0370-2693(94)91176-2
34. A. Abele et al., A Study of f0 (1500) decays into 4 pi0 in anti-p p –> 5 pi0 at rest. Phys. Lett. B **380**, 453–460 (1996). https://doi.org/10.1016/0370-2693(96)00574-6
35. B. Efron, R. Tibshirani, *An Introduction to the Bootstrap* (Chapman and Hall/CRC, New York, 1993)
36. G. Köpp, Dispersion calculation of the transition form-factor f(pi omega gamma)(t) with cut contributions. Phys. Rev. D **10**, 932–940 (1974). https://doi.org/10.1103/PhysRevD.10.932
37. S.P. Schneider, B. Kubis, F. Niecknig, The $\omega - > \pi^0\gamma^*$ and $\phi - > \pi^0\gamma^*$ transition form factors in dispersion theory. Phys. Rev. D **86**, 054013 (2012). https://doi.org/10.1103/PhysRevD.86.054013. arXiv:1206.3098
38. R. Karplus, C.M. Sommerfield, E.H. Wichmann, Spectral representations in perturbation theory. 1. Vertex function. Phys. Rev. **111**, 1187–1190 (1958). https://doi.org/10.1103/PhysRev.111.1187
39. W. Lucha, D. Melikhov, S. Simula, Dispersion representations and anomalous singularities of the triangle diagram. Phys. Rev. D **75**, 016001 (2007). https://doi.org/10.1103/PhysRevD.75.016001. [Erratum: Phys.Rev.D 92, 019901 (2015)]. arXiv:hep-ph/0610330
40. M. Hoferichter, G. Colangelo, M. Procura, P. Stoffer, Virtual photon-photon scattering. Int. J. Mod. Phys. Conf. Ser. **35**, 1460400 (2014). https://doi.org/10.1142/S2010194514604001. arXiv:1309.6877
41. D.A.S. Molnar, I. Danilkin, M. Vanderhaeghen, The role of charged exotic states in $e^+e^- \to \psi(2S)\ \pi^+\pi^-$. Phys. Lett. B **797**, 134851 (2019). https://doi.org/10.1016/j.physletb.2019.134851. arXiv:1903.08458
42. M. Jacob, G.C. Wick, On the general theory of collisions for particles with spin. Annals Phys. **7**, 404–428 (1959). https://doi.org/10.1016/0003-4916(59)90051-X
43. O. Babelon, J.L. Basdevant, D. Caillerie, M. Gourdin, G. Mennessier, Meson pair production in two-photon processes. Nucl. Phys. B **114**, 252–270 (1976). https://doi.org/10.1016/0550-3213(76)90588-5
44. D. Morgan, M.R. Pennington, Is low-energy $\gamma\gamma \to \pi^0\pi^0$ predictable? Phys. Lett. B **272**, 134–138 (1991). https://doi.org/10.1016/0370-2693(91)91025-Q (**[Erratum: Nucl. Phys. B 376, 444–444 (1992)]**)
45. R. García-Martín, B. Moussallam, MO analysis of the high statistics Belle results on $\gamma\gamma \to \pi^+\pi^-, \pi^0\pi^0$ with chiral constraints. Eur. Phys. J. C **70**, 155–175 (2010). https://doi.org/10.1140/epjc/s10052-010-1471-7. arXiv:1006.5373
46. M. Hoferichter, C. Ditsche, B. Kubis, U.-G. Meißner, Dispersive analysis of the scalar form factor of the nucleon. JHEP **06**, 063 (2012). https://doi.org/10.1007/JHEP06(2012)063. arXiv:1204.6251
47. E. Omnès, On the Solution of certain singular integral equations of quantum field theory. Nuovo Cim. **8**, 316–326 (1958). https://doi.org/10.1007/BF02747746
48. J.F. Donoghue, J. Gasser, H. Leutwyler, The Decay of a Light Higgs Boson. Nucl. Phys. B **343**, 341–368 (1990). https://doi.org/10.1016/0550-3213(90)90474-R
49. P. Buettiker, S. Descotes-Genon, B. Moussallam, A new analysis of pi K scattering from Roy and Steiner type equations. Eur. Phys. J. C **33**, 409–432 (2004). https://doi.org/10.1140/epjc/s2004-01591-1. arXiv:hep-ph/0310283
50. D.H. Cohen, D.S. Ayres, R. Diebold, S.L. Kramer, A.J. Pawlicki, A.B. Wicklund, Amplitude Analysis of the K- K+ System Produced in the Reactions pi- p –> K- K+ n and pi+ n –> K- K+ p at 6-GeV/c. Phys. Rev. D **22**, 2595 (1980). https://doi.org/10.1103/PhysRevD.22.2595
51. A. Etkin et al., Amplitude Analysis of the K0(s) K0(s) System Produced in the Reaction pi- p –> K0(s) K0(s) n at 23-GeV/c. Phys. Rev. D **25**, 1786 (1982). https://doi.org/10.1103/PhysRevD.25.1786
52. D.L. Yao, P. Fernandez-Soler, M. Albaladejo, F.K. Guo, J. Nieves, Heavy-to-light scalar form factors from Muskhelishvili-Omnès dispersion relations. Eur. Phys. J. C **78**(4), 310 (2018). https://doi.org/10.1140/epjc/s10052-018-5790-4. arXiv:1803.03171
53. M. Mai, P.C. Bruns, B. Kubis, U.-G. Meißner, Aspects of meson-baryon scattering in three and two-flavor chiral perturbation theory. Phys. Rev. D **80**, 094006 (2009). https://doi.org/10.1103/PhysRevD.80.094006. arXiv:0905.2810
54. U.-G. Meißner, S. Steininger, Baryon magnetic moments in chiral perturbation theory. Nucl. Phys. B **499**, 349–367 (1997). https://doi.org/10.1016/S0550-3213(97)00313-1. arXiv:hep-ph/9701260

55. U. Sauerwein, M.F.M. Lutz, R.G.E. Timmermans, Axial-vector form factors of the baryon octet and chiral symmetry. Phys. Rev. D **105**(5), 054005 (2022). https://doi.org/10.1103/PhysRevD.105.054005
56. F.-K. Guo, X.-H. Liu, S. Sakai, Threshold cusps and triangle singularities in hadronic reactions. Prog. Part. Nucl. Phys. **112**, 103757 (2020). https://doi.org/10.1016/j.ppnp.2020.103757. arXiv:1912.07030
57. C. Ditsche, M. Hoferichter, B. Kubis, U.-G. Meißner, Roy-Steiner equations for pion-nucleon scattering. JHEP **06**, 043 (2012). https://doi.org/10.1007/JHEP06(2012)043. arXiv:1203.4758
58. T. Ledwig, J. Martin Camalich, L. S. Geng, M. J. Vicente Vacas, Octet-baryon axial-vector charges and SU(3)-breaking effects in the semileptonic hyperon decays. Phys. Rev. D 90(5), 054502 (2014). https://doi.org/10.1103/PhysRevD.90.054502 arXiv:1405.5456
59. J.A. Oller, M. Verbeni, J. Prades, Meson-baryon effective chiral lagrangians to O(q**3). JHEP **09**, 079 (2006). https://doi.org/10.1088/1126-6708/2006/09/079. arXiv:hep-ph/0608204
60. M. Frink, U.-G. Meißner, On the chiral effective meson-baryon Lagrangian at third order. Eur. Phys. J. A **29**, 255–260 (2006). https://doi.org/10.1140/epja/i2006-10105-x. arXiv:hep-ph/0609256
61. V. Pascalutsa, R. Timmermans, Field theory of nucleon to higher spin baryon transitions. Phys. Rev. C **60**, 042201 (1999). arXiv:nucl-th/9905065, https://doi.org/10.1103/PhysRevC.60.042201